A COMPACT CIRCULARLY POLARIZED MONOPULSE SLOTTED WAVEGUIDE ARRAY FOR AIRBORNE APPLICATIONS

A Thesis

by

Wasim Nawaz

Submitted to the
Graduate School of Sciences and Engineering
In Partial Fulfillment of the Requirements for
the Degree of

MS Electrical & Electronics Engineering

in the
Department of Electrical and Electronics Engineering

Özyeğin University
October 2019

A COMPACT CIRCULARLY POLARIZED MONOPULSE SLOTTED WAVEGUIDE ARRAY FOR AIRBORNE APPLICATIONS

Approved by:

Professor Dr. Murat Uysal, Advisor
Department of Electrical and Electronics Engineering
Özyeğin University

Asst. Professor Dr. Kadir Durak
Department of Electrical and Electronics Engineering
Özyeğin University

Asst. Professor Dr. Ahmed Akgiray, Co-Advisor
Department of Electrical and Electronics Engineering
Özyeğin University

Assoc. Professor Dr. Tansal Güçlüoğlü
Department of Electrical and Electronics Engineering
Yildiz Technical University

Date Approved: 24^{th} October 2019

Asst. Professor Dr. Evşen Yanmaz Adam
Department of Electrical and Electronics Engineering
Özyeğin University

To My Beloved Family.....

ABSTRACT

In modern radar and communication systems, high gain, high power capability and low-profile antenna systems are frequently utilized. In airborne and space borne applications, slotted waveguide antenna array is widely used due to its rigid structure , low-loss and high power handling capability.

In this thesis, a compact, lightweight, high reflection bandwidth, high gain and circularly polarzied slotted waveguide array antenna with monopulse capability operating in Ku-band is presented. Target application of this antenna is radio links on airborne platforms with built-in tracking capability . This thesis is divided into two parts: 1) Design of compact standing wave slotted array; 2) Design of a low-cost linear polarization (LP) to circular polarzition (CP) converter.

In the first part of thesis, an antenna system is presented that has two key components: monopulse comparator/feed network and antenna section. The antenna is designed at 15 GHz and simulated using ANSYS HFSS. It is a planar array of 6x8 radiating slots with a gain greater than 22.5 dB at 15 GHz , side-lobe level (SLL) $\leq$ 13 dB , reflection bandwidth of 1200 MHz. Monopulse comparator network is Magic Tee based waveguide structure. The antenna has maximum dimension of $10.8\,\text{cm} * 10.7\,\text{cm} * 4\,\text{cm}$ that makes it easy to house on an aircraft.

In the second part of thesis, a LP to CP polarizer is presented. The proposed polarizer is a multi-layer metasurface based structure that converts incident linearly polarized wave into circularly polarized wave. The polarizer presented in this thesis is based on meander line and strip line hybrid concept. Each substrate layer is rotated 45° with respect to previous layer and is seperated by low permittivity material called spacer. The unit cell of the polarizer is square in shape with dimensions of

5.1 mm ∗ 5.1 mm. Its axial ratio bandwidth is 2 GHz i.e: axial ratio is less than 3-dB from 14-16 GHz . It is also low-cost as compared to the available literature because thick substrates are used instead of high cost thin substrate and also one substrate layer is based on FR-4 laminate.

Keywords: Monopulse, Slotted Waveguide, Magic-Tee, Polarizer

ÖZETÇE

Modern radar ve iletişim sistemlerinde, yüksek kazanç, yüksek güç kapasitesi ve düşük profilli anten sistemleri sıklıkla kullanılmaktadır. Havadan ve yere dayalı uygulamalarda, rijit yapısı, düük kaybı ve yüksek gü kullanma kabiliyeti nedeniyle oluklu dalga kılavuzu anten dizisi yaygın olarak kullanılmaktadır.

Bu tez çalımasında, Ku-bandında çalıan monopuls yeteneğine sahip kompakt, hafif, yüksek yansıma bant geniliği, yüksek kazan ve dairesel polarize oluklu dalgalı dalga dizisi anten sunulmaktadır. Bu antenin hedef uygulaması, yerleik izleme özelliğine sahip havadaki platformlardaki radyo baǵlantılarıdır. Bu tez iki bölüme ayrılmıştır: 1) Kompakt duraǵan dalga oluklu dizisinin tasarımı; 2) Düük maliyetli bir doürusal polarizasyon (LP) ile dairesel polarizasyon (CP) dönütürücüsünün taşarımı.

Tezin ilk bölümünde, iki ana bileşene sahip bir anten sistemi sunulmuştur: monopuls karşılatırıcı besleme aǵı ve anten bölümü. Anten 15 GHz'de tasarlanmış ve ANSYS HFSS kullanılarak simüle edilmiştir.15 GHz, yan lob seviyesi (SLL) 13 dB'de 22.5 dB' den daha fazla kazancı olan 6x8 yayılan olukların düzlemsel bir dizisidir.,1200 MHz yansıtma bant genişliği. Monopuls karşılaştırıcı aǵı, Magic Tee tabanlı dalga kılavuzu yapısıdır. Anten, uçakta yerletirmeyi kolaylatıran maksimum 10.8 x 10.7 x 4 cm boyutuna sahiptir.

Tezin ikinci bölümünde, bir LP-CP polarizörü sunulmuştur. Önerilen polarizer, olayı doǵrusal polarize dalgayı dairesel polarize dalgasına dönüştüren çok katmanlı bir metasurface bazlı yapıdır. Bu tezde sunulan polarizer, kıvrımlı ve düz çizgi hibrid konseptine dayanmaktadır. Her bir substrat katmanı önceki katmana göre 45° döndürülür ve aralayıcı adı verilen düük geirgenlik materyali ile ayrılır. Polarizörün birim hücresi, 5.1 mm x 5.1 mm boyutlarında kare eklindedir. Eksenel oran bant

geniliği 2 GHz'dir, yani eksenel oran 14-16 GHz'den 3-dB'den azdır. Aynı zamanda, mevcut literatüre kıyasla düşük maliyetlidir, çünkü yüksek maliyetli ince substrat yerine kalın substratlar kullanlr ve ayrca bir substrat tabakası FR-4 laminat esaslıdır.

ACKNOWLEDGEMENTS

I have had an honour of working with Dr. Ahmed Akgiray, my advisor during graduate studies. I am really thankful to his kind support throughout my research. I have gained a lot of knowledge in the field of Electromagnetics from his experience, research methodology and expertise. Indeed, he played a crucial role to successfully achieve my goals during this research.

I would like to express my gratitude to Prof. Dr. Murat Uysal, Assoc. Prof. Dr. Tansal Güçlüoǵlü, Asst. Prof. Dr. Evşen Yanmaz Adam and Asst. Prof. Dr. Kadir Durak for finding time in their busy schedules to constitute my thesis committee. A bundle of thanks to Mr. A.K.M Shafaat Ali for his guidance and support throughout my degree. I am also very thankful to my friend Wazir Akbar whose support particularly towards the end of my degree really helped me to achieve my goals. Thanks to Mert Karaca from Electronics Lab for all his technical support during lab sessions.

My words cannot express my feelings for my late father who was always a great support in my life and his lessons will be always a source of guidance for me. To my mother and siblings, thanks for being a such great family. Last but not least, bunch of thanks to my better half Ayesha , for all the encouragement and support. I really appreciate your efforts for brightening my world and for being an important part of my story.

TABLE OF CONTENTS

LIST OF TABLES

LIST OF FIGURES

CHAPTER I

INTRODUCTION

The last few years has seen a tremendous increase in use of unmanned aerial systems (UASs) in civilian and military applications [1, 2, 3, 4, 5, 6]. UASs, also known as unmanned aerial vehicles (UAVs) and drones, come in variety of sizes and capabilities with different payload capacities. Primary civilian use case of UASs is scientific exploration of natural phenomenon such as vegetation and soil measurements, atmospheric and weather research as well as tracking man-made events (fire, land use, etc.). In the military domain, UASs are used for aerial surveillance, air and ground target detection & tracking, and in some cases aerial delivery of bombs [7, 8, 9, 10].

While no standard classification exists that covers all UASs from the smallest drone to the Global Hawk to the US Air Forces X71B space UAS, the antenna design presented in this thesis is primarily intended for so called Medium Altitude Long Endurance (MALE) and High Altitude Long Endurance (HALE) UASs. MALE & HALE drones are classified as drones with weight $>$ 600 Kg [11]. MALE drones have normal operating altitude up to 45,000 ft and can stay in air from 5 to 24 hours. Most common examples are Shadow 600 and Bayraktar TB2 as shown in Fig.1.On the other hand, HALE drones have normal flight altitude up to 65,000 ft above ground level and can stay airborne for more than 24 hours. Examples include Predator B and Global HAWK etc as shown in Fig.2

MALE and HALE UAVs are generally equipped with payloads to carry out intelligence, surveillance, target acquisition and reconnaissance (ISTAR) missions. These payloads includes optical payload such as electro-optic(EO), forward looking infrared(FLIR) and laser range finder (LRF) as well as synthetic aperture radar (SAR)

a) b)

Figure 1: MALE UAVs a) Bayraktar TB2 b) Shadow 600

a) b)

Figure 2: HALE UAVs a) Global Hawk b) Predator B

payload such as ground moving target indicator (GMTI) and inverse SAR (ISAR). Payload carrying capacity of MALE UAVs is from few kg to 600 Kg. For example, MALE class UAVs Shadow and Predator have payload capacity of 75 Kg and 600 Kg respectively[12]. HALE UAVs have payload capacity ranging from few hundred to few thousand Kg. For instance, Global Hawk & Predator B have payload capacity of 900 Kg and 3000 Kg respectively[12].

A UAS data link typically consists of an RF transmitter and a receiver, an antenna, and modems to interface these parts with the sensor systems. For UAS, data links serve two important functions:

1. Uplinks from the ground station and/or a satellite to send control data to the UAV

2. Downlinks from the UAV to send data from the onboard sensors and telemetry

system to the ground station

Command , control and communication of MALE and HALE UAVs are divided into two main RF Line of sight (LOS) and beyond line of sight (BLOS) communications. LOS is type of communication that is performed only when onboard antenna and ground station antenna are pointing towards each other. BLOS is type of radio communications that is either too far or fully obscured by terrain. Uplink and downlink data links are performed using LOS while Air Traffic Control (ATC) is BLOS [13, 14, 15].

These communications are done primarily through the use of RF applications, usually, satellite communication links in UAS are used either in LOS (for military applications) or in BLOS mode. The most common frequency bands of this type of links are [13, 15, 16]:

- X band (8-12 GHz): military applications with high data rate
- Ku band (12-18 GHz): historically used for high speed links. Higher propagation losses but high penetration power due to shorter wavelength
- K band(18-26.5 GHz): possesses a large frequency range which conveys large amounts of data. As a main drawback it should be mentioned that it requires powerful transmitters and it is sensitive to environmental interferences

The key motivation for this research is to design a small, robust and high performance Ku-band circularly polarized antenna with simultaneous tracking capability to be used on a MALE/HALE UAS that is wideband enough to cover both receive (uplink) and transmit (downlink) Ku-band line-of-sight communication frequency ranges. The antenna design specifications used in this research are determined by using performance parameters of some commercially available hardware as well as taking advantage of existing literature [17] and performing a link budget analysis. The link

Table 1: A simple Link budget

UAV Link budget	UAV to GND (Downlink)	GND to UAV (Uplink)
Frequency	**14.4-14.83 GHz**	**15.15-15.35 GHz**
Modulation	QPSK	QPSK
Channel bandwidth (MHz)	8	6
Bit Rate (Mbps)	10.5	3.7
Distance (Km)	250	250
Free space loss (dB)	163.82	164.12
Pointing loss (dB)	1.5	1.5
Tx Power (dBm)	40	40
Tx Cable loss(dB)	2	2
Tx Antenna gain (dB)	20	35
Rx Antenna gain(dB)	35	20
Rx Cable loss(dB)	2.5	2.5
Min. CNR requirement(dB)	8.3	2.7
Rx sensitivity at input (dBm)	-95	-100
Link margin (dB)	**20.18**	**25.48**

budget is provided in Table.1 (see Fig. 3 for path loss versus range) and below, some of the underlying assumptions are highlighted:

1. Maximum UAS range to ground station: 250 km
2. Typical UAS altitude: 15,000 to 40,000 feet
3. Transmitter output power for both UAS and ground station: 10 Watts
4. Reflector antenna of diameter 60 cm at the ground station
5. Minimum target link margin of 20 dB

   As a result of the link budget analysis, the antenna performance specifications are determined as shown in Table.2.

In UAVs, uplink is between a control ground station (CGS) and UAV for telemetry & telecommands (TTC) while downlink is for payload data transfer from onboard equipment to the ground station. As UAVs are equipped with advance optical systems

Figure 3: Variation in path loss with distance

Table 2: Design requirements for monopulse slot array

Parameter	**Value**
Frequency Band	Ku (14.4 GHz - 15.35 GHz)
Bandwidth	950 MHz
Gain	21 dB
Beam-width	10 deg
VSWR	< 2
Polarization	Circular
Axial Ratio	< 3 (dB)
Monopulse capability	Single plane (Az)

as well as SAR systems, payload data transfer rate is desired to be higher than uplink. In this application, 14.4 - 14.83 GHz frequency range is used as a downlink while 15.15 - 15.35 GHz is used as an uplink frequency range. Due to higher data rate requirement for payload data transfer, downlink bandwidth is desired to be higher than uplink.

Slotted waveguide arrays are frequently used in airborne applications but available designs have certain limitations such as lack of monopulse capability [18, 19] or monopulse antenna with more weight and volume[20, 17]. The presented antenna has advantage of being low-weight , compact and high gain with impedance bandwidth greater than 1200 MHz. It has monopulse capability in single plane (azimuth) because desired application requires only one plane monopulse capability. Table.3 presents a comparison between available designs and current design. Smaller size can be classified as few inches, medium more than 10 inches and large greater than 50 inches.

Table 3: Comparison with other designs

Design	**Monopulse**	**Polarization**	**Size**	**Bandwidth (%)**
Li et.al	No	Linear	Small	2
Ya-Qing et.al	No	Linear	Medium	17
Hendrik Bayer et.al	Yes (Dual plane)	Circular	Very large	20
CPII (Commercial)	Yes (Dual plane)	Circular	Small	6.3
Current design	Yes (Az plane)	Circular	Small	8

Thesis structure is as:

The thesis begins with the introduction and theoretical analysis of slotted waveguide antenna arrays in chapter 2. A brief introduction to different methods of excitation for the slot arrays and design of planar slot array antenna with a gain greater than 20 dB is also presented in chapter 2. Chapter 3 begins with the analysis and design of a wideband monopulse comparator network.Design based on Magic Tee based network is presented. In Chapter 4, results of complete structure i.e: antenna

with monopulse comparator network are presented. The analysis, design and results of the a polarization converter with capability of converting incident linearly polarized wave to a circular polarized wave in the desired frequency range (14.4-15.35 GHz) is presented in Chapter 5. Thesis concludes with conclusion and future work in chapter 6.

CHAPTER II

SLOTTED WAVEGUIDE ANTENNA

Simple geometry,high radiation efficiency and easy installation make slotted waveguide antenna arrays suitable for airborne, spaceborne, radar communications and other high performance applications. Slots can be etched in the waveguide to get desired radiation pattern. The slots arrays can be excited from edge or centre. For a slotted waveguide array, different types of feed networks are used such as corporate feed networks, monopulse comparator network and substrate integrated waveguide based netwrok. Choice of the feed network mainly depends upon the application requirements and constraints. Slotted waveguide arrays can be either standing wave or travelling wave arrays depending on application. Former is desired in applications with boresight beam requirement and later is employed for applications with tilted beam requirements. The main disadvantage of using standing wave arrays for tracking radar applications is small reflection bandwidth [21].

High frequency radiation from resonant slots was first presented by Watson in [22] and analytical study for radiating slots in rectangular waveguides was carried out by Stevenson in [23]. Watson laid the foundation for the theory of resonant coupling slots and explained how slots can be utilized to couple waveguides. Stevenson investigated extensively the launch of high frequency radiation from resonant slots in the form of transmission line model. R.S Elliot et.al extended the Stevenson's method and presented the theory of small slot arrays in [24]. A travelling wave shunt slotted array having main beam offset from the bore-sight and spacing between the slots not equal to $\lambda/2$ was presented by R.S Elliot in [25]. M. Orefice and R.S Elliot presented analysis of radiation from longitudinal slots cut in the broadside of waveguide in [26]. This

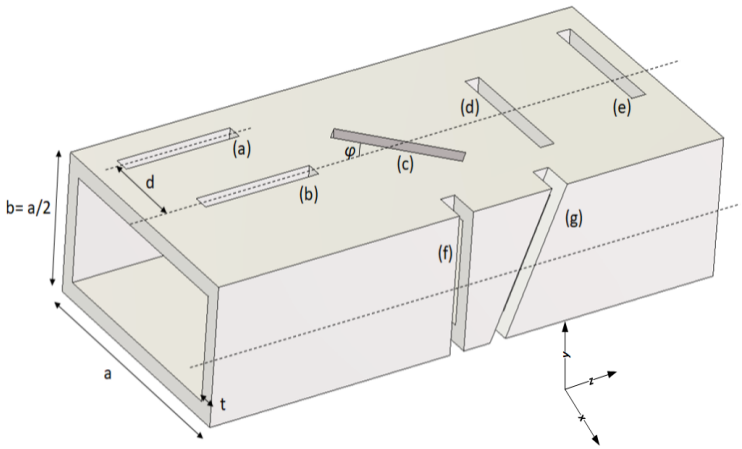

Figure 4: Different types of slots cut in waveguide

analysis helps in exciting radiating waveguides via coupling waveguides through an inclined slot common to broadside of both waveguides. Yee in [27] included the effect of offset from centre line on longitudinal shunt slot arrays. Later, R.S Elliot presented a detailed and improved procedure for the design of slotted waveguide arrays with longitudinal shunt radiating slots in the broadside of waveguide in [28]. Josefsson in [29] presented a moment method based solution to accurately compute the admittance of longitudinal slots to determine the resonant length of the slots. As standing wave slotted arrays exhibit small impedance bandwidth, Muller in [30] devised a method to increase the bandwidth by feeding the array from centre using coupling slot instead of end-fed approach. His approach resulted in increased bandwidth but radiation pattern was degraded because in resonant arrays slots are placed at the maxima of the standing wave.

There are different types of slots that can be etched in the waveguide as shown in Fig.4. It can be seen that slots can be cut either in the broadside or vertical wall of the rectangular waveguide.

The labels depicted in Fig. 4 are explained below :

1. Slots

(a) Longitudinal shunt slot offset centre

(b) Longitudinal shunt slot at centre

(c) Inclined slot at an angle ϕ with respect to centre

(d) Series slot at centre

(e) Series slot offset from centre

(f) Vertical slot

(g) Vertical inclined slot

2. Waveguide dimensions

(a) Broadside dimension (Width)

(b) Narrow side dimension (Vertical height)

(c) Side wall thickness (t)

Slots a, b, g and f are shunt slots because they interrupt the surface currents Jx, Jy and can be represented by equivalent shunt admittance while slots d, e and f are series slots as they interrupt the transverse current Jz and can be represented by equivalent series impedance. Slot "b"does not radiate because of the zero transverse current. Also, slot "f"does not radiate because its direction is parallel to the side wall current.

Longitude shunt slots are most commonly used when broadside beam is desired in waveguide antenna arrays. The slot parameters and its equivalent shunt circuit model given in [31] is shown in Fig. 5. Slot length is usually selected as $0.5\lambda_\circ$ and slot width as $0.1\lambda g$ where $\lambda_\circ$ and λg are free space and guide wavelengths respectively.

The slot array antennas are generally excited with fundamental TE_{10} mode and end walls of the waveguide are terminated with either short circuit or matched impedance. If slot array is excited with dominant TE_{10} mode of the rectangular

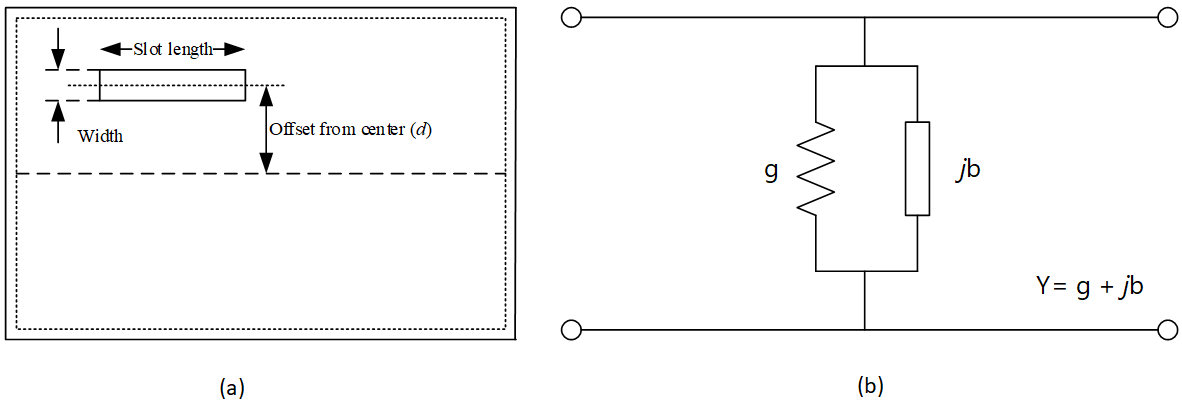

Figure 5: (a)Longitudinal shunt slot (b) Equivalent Circuit representation

waveguide, the E-field is given by Eq. 1 [31]

$$E_y = E_\circ sin(\beta_x x) e^{-j\beta_z z} \tag{1}$$

where β_x and β_z are given by Eq.2.

$$\begin{aligned} \beta_x &= \pi/a \\ \beta_z &= 2\pi/\lambda_g \\ \lambda_g &= \frac{\lambda}{\sqrt{\lambda_c^2 - \lambda^2}} \\ \lambda_c &= 2a \end{aligned} \tag{2}$$

λ_g is the guided wavelength, z is the direction of propagation of wave,λ_c is the cut-off wavelength and λ is the free space wavelength.

2.1 Types of Slotted Waveguide Array

Slotted waveguide arrays are mainly categorized as travelling wave slot array (TWSA) and standing wave slot array (SWSA). Travelling wave arrays generally have higher bandwidth [21] as compared to standing wave slot arrays. TWSA are prefer in applications where direction of main beam is desired at certain angle from bore-sight On the other hand, SWSA always radiates broadside. The main difference between TWSA and SWSA are explained in the following subsections

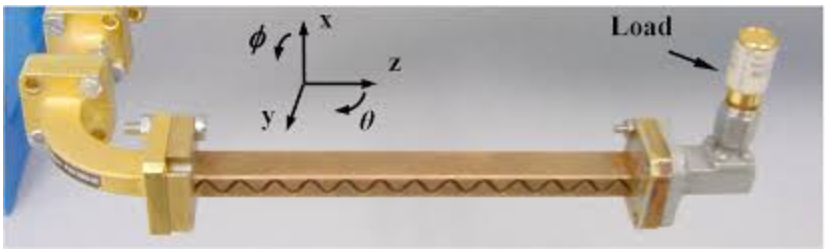

Figure 6: Travelling wave slot array with a matched load

2.1.1 Travelling Wave Slot Array (TWSA)

Travelling wave slot arrays are employed in applications where frequency scanning or the direction of main beam pointed at certain angle from bore-sight is desired. They are always excited from edge and inter slot spacing can vary between slots. In design of TWSA , inter-slot spacing can be slightly greater or less than $\lambda_g/2$ but should not be $\lambda_g/2$. In order to increase bandwidth of TWSA, slots are designed as resonant slots i.e: they are resonant at the centre frequency. As TWSA are always edge fed, therefore the amplitude of wave decreases towards end because of energy coupling by radiating slots. The typical narrow wall TWSA by [32] is shown in Fig.6

2.1.2 Standing Wave Slot Array (SWSA)

Standing wave slot arrays (SWSA) are used in applications with broadside beam direction requirements. Unlike TWSA, SWSA exhibits narrow impedance bandwidth due to dispersions inside the waveguide because of slots position at maxima of the standing wave. Planar SWSA can be designed easily by stacking linear array sticks next to each other. Inter-slot spacing in SWSA is always $\lambda_g/2$ where λ_g is the guide wavelength at centre frequency. Because of $\lambda_g/2$ spacing, fields inside the waveguide repeats at $\lambda_g/2$ but out of phase. Therefore , in order to excite all slots in phase, they are placed at alternate positions with respect to waveguide centre. They can be excited either from edge or centre. When excited from centre, the edge walls should be terminated with a short circuit placed at $\lambda_g/4$ or $3\lambda_g/4$ spacing from the last

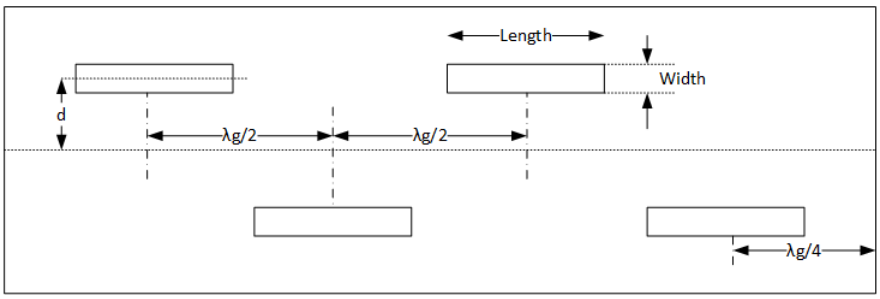

Figure 7: Standing wave slot array

slot. Inclined slots are generally used to couple power from feed section to radiating waveguide section. A typical SWSA with different design parameters is shown in Fig.7

2.2 Design of Standing Wave Slot Array

The initial design of slot array antenna is based on the theory presented by Stevenson in [23] and R.S Elliot in [24]. Design frequency is set as 15 GHz to obtain the required length and width of the radiating slot.The design is based on longitudinal shunt slots cut in the broad side of the waveguide. The presented antenna is an array of 6x8 slot elements based on standing wave slot array concept as shown in Fig.11.

The designed antenna has three main components named as input , coupling and radiating waveguides:

1. **Input Waveguides:** The first component is the excitation or input waveguides to the antenna. There are two input waveguides that are designed using standard WR-61 rectangular waveguide with an inclined slot to couple input power to the coupling waveguides. When waveguide array is excited from centre using an inclined slot, power coupled from slots can be controlled by rotating angle of the slots with respect to centre. According to Roland A. Gilbert[31], power is proportional to $Sin^2(\phi)$ where ϕ is the angle of inclined slot with centre axis. In order to get the desired impedance bandwidth, inductive irises are used

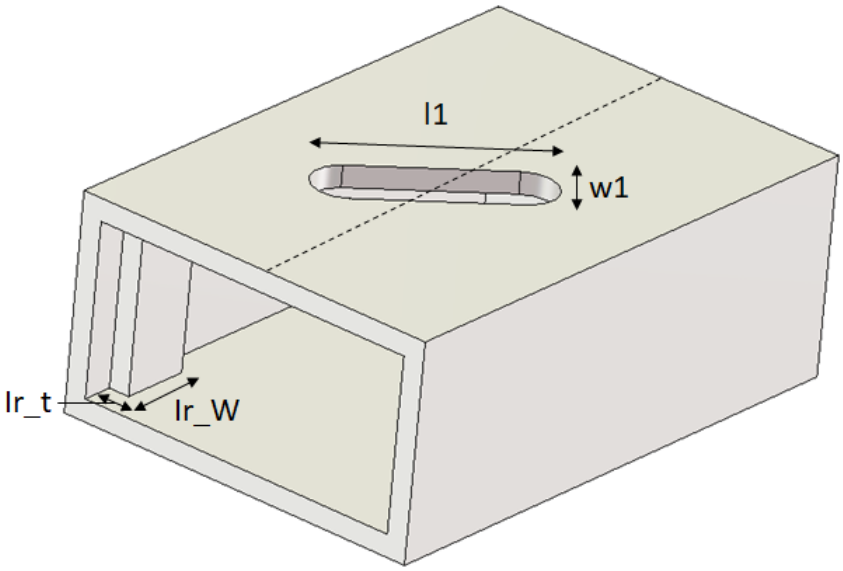

Figure 8: Input Waveguide

in input waveguides. The design parameters of input waveguide are shown in Fig.8 and tabulated in Table.4

2. **Coupling Wavguides:** The second component of antenna is coupling waveguides that couple energy from input waveguides to the radiating waveguides. There are two coupling waveguides with six inclined slot each. These are also standard WR-61 rectangular waveguides. In order to couple uniform energy to all radiating waveguides, slots are placed at a distance equal to the width of the radiating waveguide so that radiating waveguides can be excited from centre. Inclined coupling slots are used with initial length and width equal to $\lambda/2$ and $0.05\lambda_g/2$ respectively which are later tuned to get the best results. The design parameter of coupling waveguide are tabulated in Table.5

3. **Radiating Wavguides:** The third and most critical component of this antenna array is the radiating section. Different approached were analysed to get the desired electrical performance. In the first phase, an array in the form of 3x8 is

Table 4: Input Waveguide parameters

Parameter	**Value (mm)**
Length	25.8
Width	15.7988
Height	7.8994
Thickness	1
Iris width(Ir_w)	3
Iris thickness (Ir_t)	1
Slot length(l1)	10
Slot width(w1)	3
Slot angle	45 deg

Table 5: Coupling Waveguide parameters

Parameter	**Value (mm)**
Length	106
Width	15.7988
Height	7.8994
Thickness	1
Slot length	9.85
Slot width	0.9
Slot angle	34 deg

Table 6: Radiating linear array parameters

Parameter	**Value (mm)**
Length	52
Width(w)	15.7988
Height(l)	7.8994
Thickness(t)	1
Slot length(S_l)	9.85
Slot width(S_w)	1.4
Offset(d)	1.8
Slot Spacing	$\lambda_g/2$

designed with two sections of three 1x4 sub-arrays. Each section was separated from other with a certain distance to get better isolation. This has a simulated gain of 20 dB as required but no margin for manufacturing losses. Therefore, another array with high gain is designed with a gain greater than 22.5 dB at 15 GHz. This provides a margin for manufacturing. There are total twelve 1x4 linear arrays that are placed next to each other to constitute a planar array of 6x8 radiating slots. These are longitudinal slots etched on the broadside of the waveguide to get the desired radiation pattern. It is worth mentioning that antenna is designed keeping in view manufacturing for realization of proposed design. Initially, radiating slots were rectangular which were tuned for rounded corners. Also, aperture is designed separately from radiating waveguides. This helped to analyse the effect of aperture gap from radiating waveguides. It is observed that up to 50 μm gap between aperture and radiating waveguides can be tolerated during assembly process of the antenna. Slots have length and width of $\lambda/2$ and $0.05\lambda_g/2$ respectively. Inter slot spacing is kept $\lambda_g/2$ throughout the array and distance of last slot from the short wall is $\lambda_g/4$. The design parameter of the radiating section linear array are shown in Fig.9 and are tabulated in Table.6

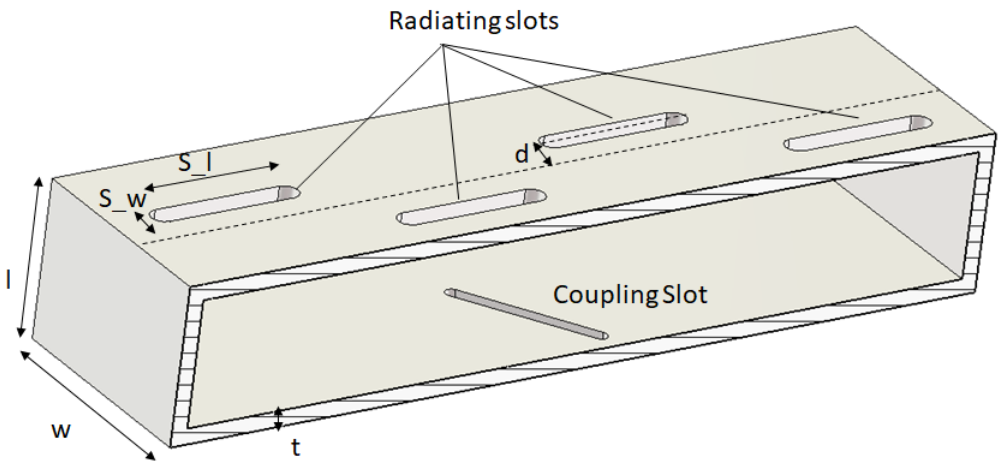

Figure 9: Cross section of 1x4 linear array

Coetzee et.al presented detailed analysis on bandwidth enhancement using sub-array concept in [33]. According to Coetzee, phase differences in slot fields of large slot arrays occur because of the change in peaks of the standing wave from slot locations that results in frequency changes and hence limiting bandwidth. These frequency variations can be avoided by using small arrays or dividing large array in sub-arrays. Therefore, 6x8 planar array is divided into twelve 1x4 linear arrays to enhance the impedance bandwidth.These linear arrays are excited through two coupling waveguides with six inclined slots each. Each coupling waveguide is further coupled to an input waveguide to integrate the antenna to feed network.

2.3 3-D Model

The antenna is designed and simulated in commercial electromagnetic simulator HFSS [34]. The designed antenna is compact, low-profile three layer structure. Frequency domain solver of the HFSS is used. Increasing the mesh cells per wavelength give better approximation but also results in higher computation time. Therefore, 15 cells per wavelength are used to get an optimum mesh for better results. Top view of the antenna section is shown in Fig.10. Exploded view explaining different parts of the

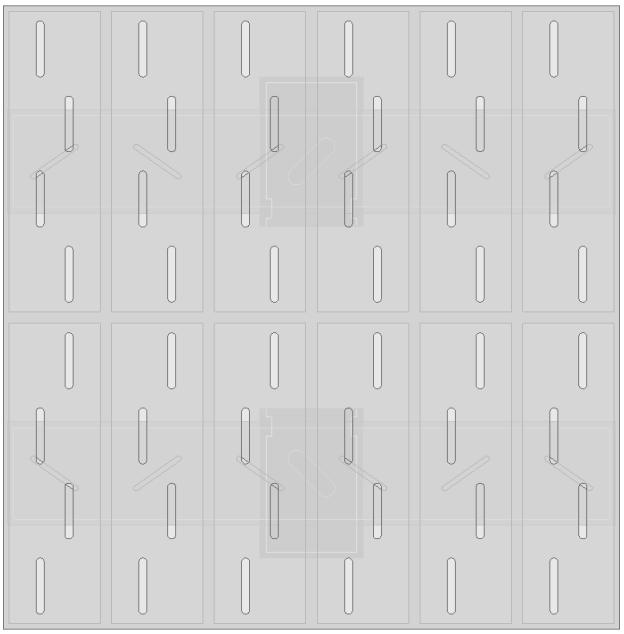

Figure 10: Top view of slot array

antenna section is shown in Fig.11

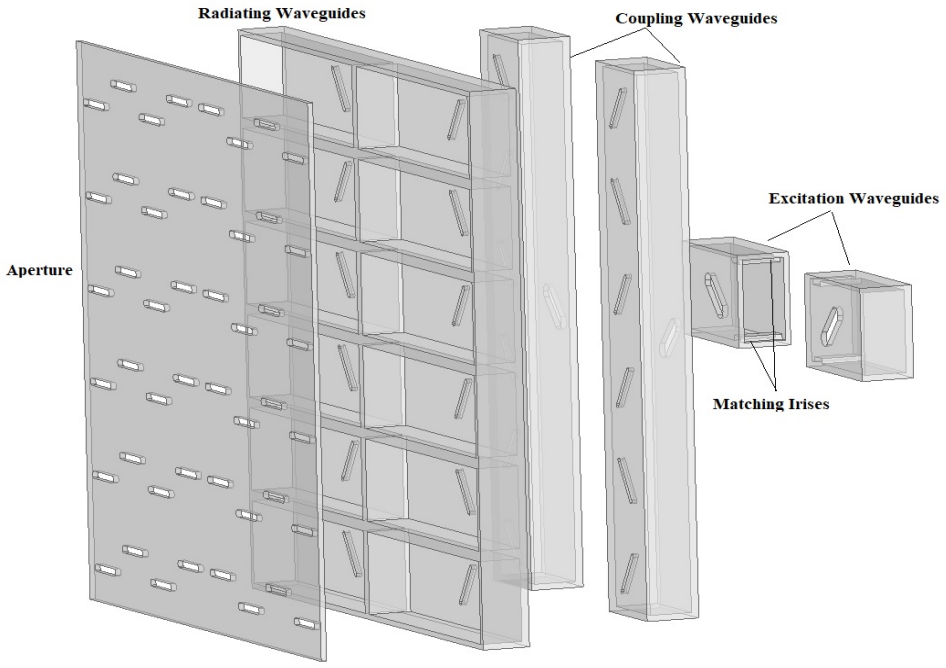

Figure 11: Exploded view of slot array

2.4 Antenna Results

The designed antenna meets all the desired performance requirements. Impedance bandwidth defines frequency band in which the impedance of antenna is matched to an input impedance. It has good impedance bandwidth of 8% (fractional bandwidth) at 15 GHz i.e: greater than 1200 MHz.Antenna gain is another key performance indicator of design. Gain is the measure of ability of an antenna to increase the power in a given direction as compared to an isotropic antenna. It has gain greater than 22.5 dB at design frequency of 15 GHz. It has side-lobe level (SLL) of -13 dB. 3 dB beam width is an indicator of antenna directivity when its gain is reduced to one-half of maximum gain. 3 dB beam width in azimuth plane is 9.3° and 10.8° for elevation plane at 15 GHz.

Reflection coefficient of an antenna depicts to which extent an antenna is matched to input impedance in the desired band. The reflection coefficient of array is shown in Fig. 12. The gain plot at design frequency of 15 GHz is shown in Fig.13. For the sake of simplicity, far-field result of antenna section is shown only on design frequency. The cross polarization level is greater than 50 dB and is shown in Fig.14. The designed array has a gain greater than 22 dB in whole downlink frequency range of 14.4-14.83 GHz. The gain of antenna in uplink frequency range i.e 15.15-15.35 GHz is greater than 20.5 dB. The gain vs frequency plot is shown in Fig.15.

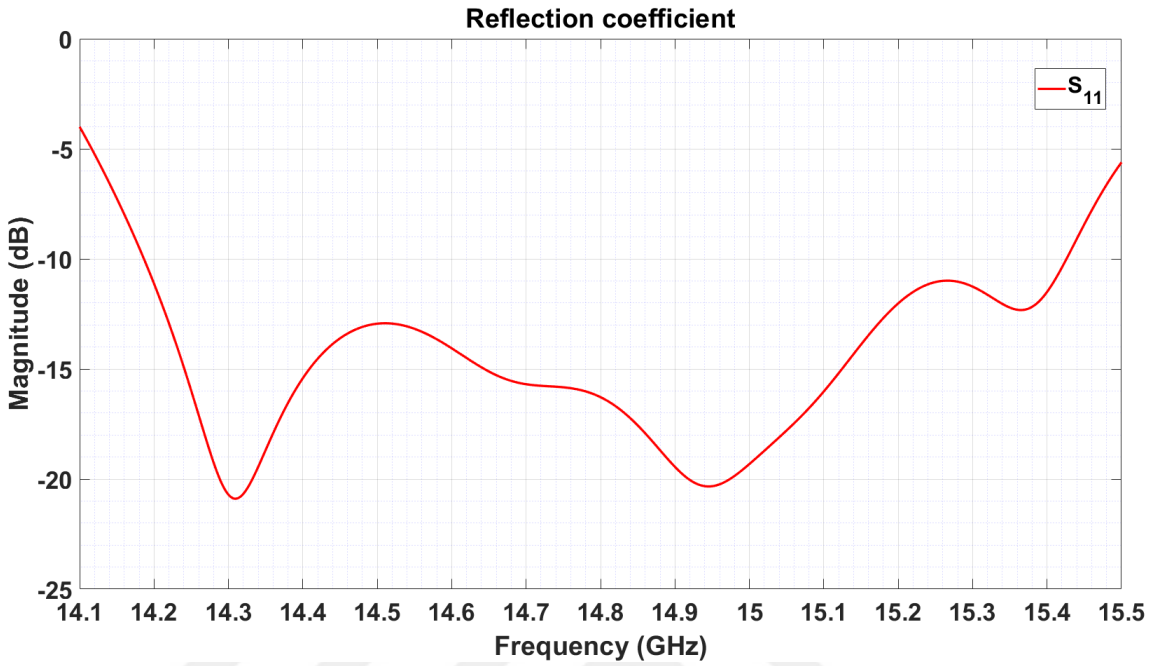

Figure 12: Reflection Coefficient of the designed array

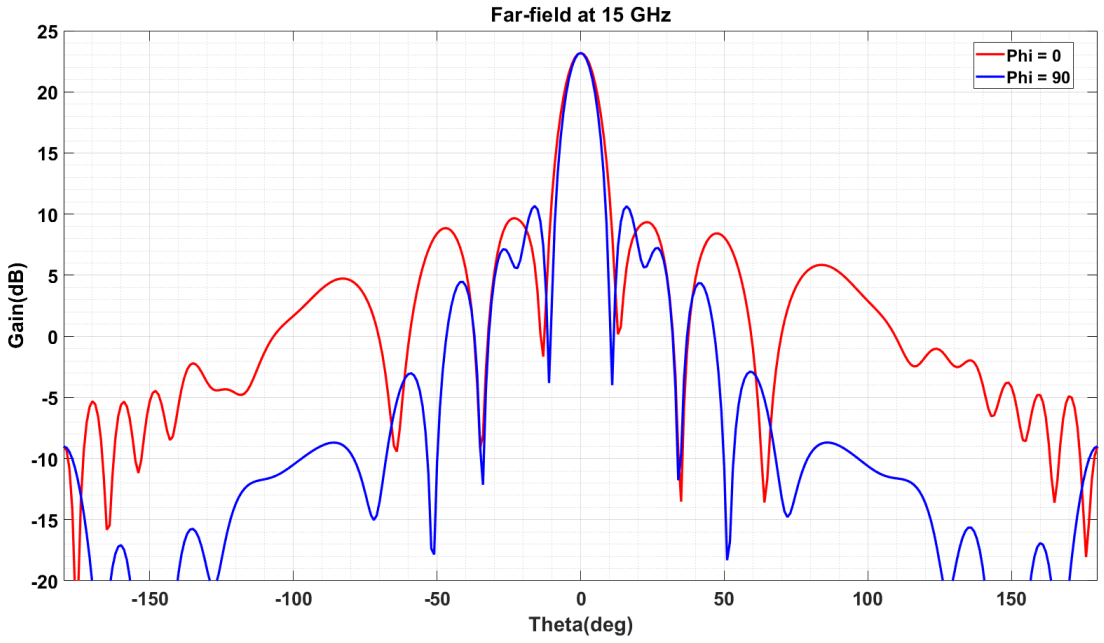

Figure 13: Gain (dB) at 15 GHz

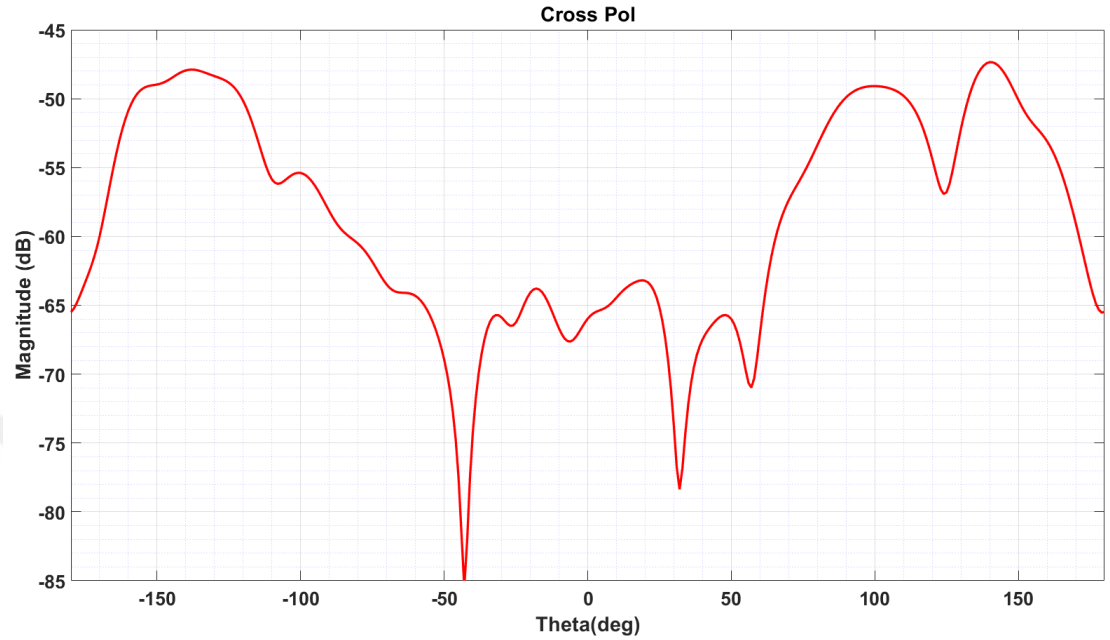

Figure 14: Cross polarization plot

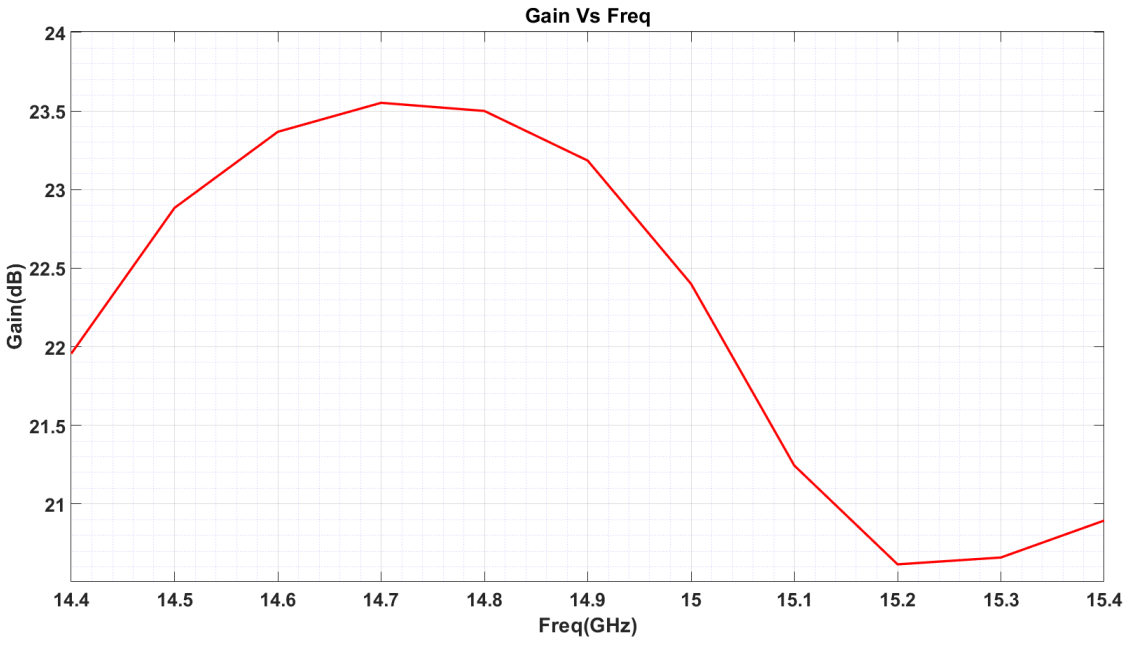

Figure 15: Gain versus frequency plot

CHAPTER III

MONOPULSE COMPARATOR NETWORK

Antenna arrays have narrow angular beam-width due to which they are widely used in tracking radar applications[35]. Mono-pulse is an efficient way to determine angular location of a target by comparing signals simultaneously received by two different antenna patterns. In radar tracking applications, waveguide fed arrays can be combined with mono-pulse comparator networks to obtain desired tracking radiation patterns known as sum and difference patterns[36, 37, 38].

The slotted waveguide antenna array can be excited in number of ways depending upon the application. When linear arrays are combined together to form a planar array, feed network is required to excite all the linear arrays. Feed network for slot array antenna can be either a microstrip based like substrate integrated waveguide (SIW) [39] or waveguide based [40]. One main advantage of using slot arrays for high performance application is that feed network can also be made of waveguides.

When slot arrays are used for UAV radio links, generally sum and difference radiation pattern of antenna is desired. This can be achieved by using monopulse comparator network so that antenna can have sum and difference radiation pattern simultaneously.

3.1 Introduction

The radiation pattern of an antenna aperture can be divided into four sub-array patterns A, B, C and D as shown in Fig. 16 . In mono-pulse antenna system, sum (Σ) Eq. 3 and horizontal difference(Δ) Eq. 4 patterns are given by

$$\Sigma = (A + B) + (C + D) \tag{3}$$

$$\Delta = (A + B) - (C + D) \tag{4}$$

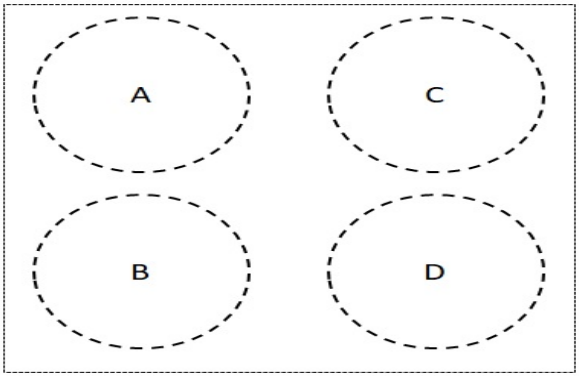

Figure 16: Illustration of four sub-patterns of an antenna to a Mono-pulse Network

Monopulse Sum and difference pattern concept is shown in Fig. 17

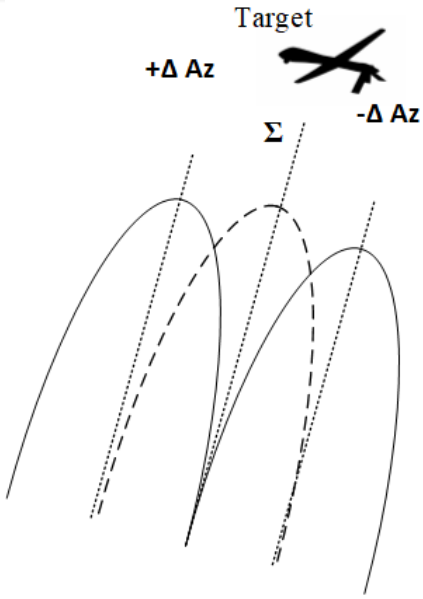

Figure 17: Sum and difference pattern illustration of Monopulse radar

Hybrid junctions based on magic Tee´s or branch line couplers are employed to combine and divide signals to achieve monopulse tracking. These hybrid junctions

have some pros and cons in terms of bandwidth, impedance matching and complex integration with radiating waveguides in a monopulse system. Comparator networks based on Magic Tee´s are widely used because they provide good isolation between output ports, easy integration behind the antenna resulting in a compact system and frequency independence of output isolation because of asymmetric even-odd modes. The only disadvantage of using magic Tee based comparator network is the mismatching of input and output ports. Iris or some other form of waveguide discontinuity is used to either reduce the effective height or effective width of the waveguide [41, 42] .

Magic Tee based monopulse comparator network is utilized to get the desired bandwidth. Magic Tee can be either planar or folded structure. A comparison of two types of Magic Tee based monopulse comparator network is presented by Guan et. al in [40]. Guan et. al suggested the use of folded type Magic Tee based comparator network instead of planar Magic Tee for wideband applications but that results in complex and difficult structure to integrate with antenna array.

3.2 Comparator Design

In this research, a Magic-tee based comparator network is used to make whole structure compact and easy to assemble. Monopulse comparator networks can provide sum and difference pattern in both principal planes. In the present application, tracking in only azimuth plane is needed. Consequently, monopulse comparator network is designed to give azimuth difference only, as opposed to elevation and azimuth difference patterns. In order to overcome the bandwidth limitation of planar magic Tee based comparator network, a waveguide discontinuity in the form of an inductive Iris and a septum is used to match both input ports of the waveguide to get the desired bandwidth. The designed comparator network is bilayer waveguide structure. Difference port is coupled with Tee through a shunt slot. This way a better isolation between sum and difference ports can be achieved. E-plane or Sum(Σ) port of the

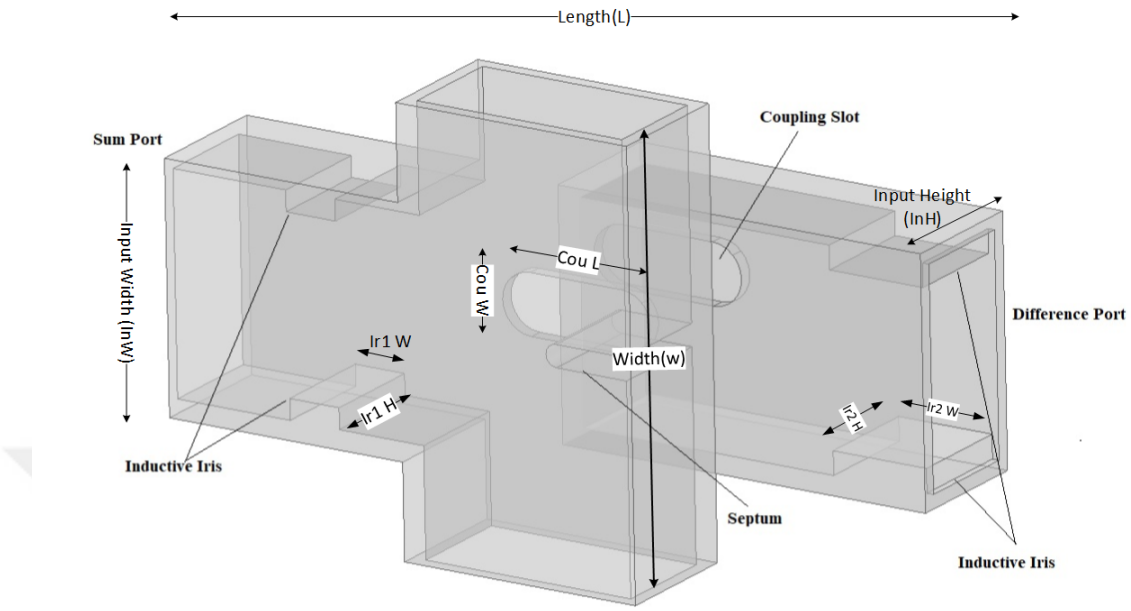

Figure 18: Semi-transparent view of Comparator Network

waveguide has relatively higher bandwidth (3 GHz) than H-plane or difference(Δ) port bandwidth (1.42 GHz) because bandwidth is limited by the width and position of the shunt coupling slot [40]. A detailed view illustrating different components of comparator network is shown in Fig.18. Inductive irises are used to get better impedance matching and bandwidth. The total height of the comparator network is only 2 cm making it suitable to integrate with antenna array and to fit on-board easily for airborne applications. Slot arrays are operated only in single mode (lowest dominant mode) to have better control over excitation. The power flow across comparator network is shown in Fig.19. It can be seen that input power is divided equally between two outputs of comparator to excite feeding section of antenna. Different design parameters illustrated in Fig.18 are tabulated in Table.7.

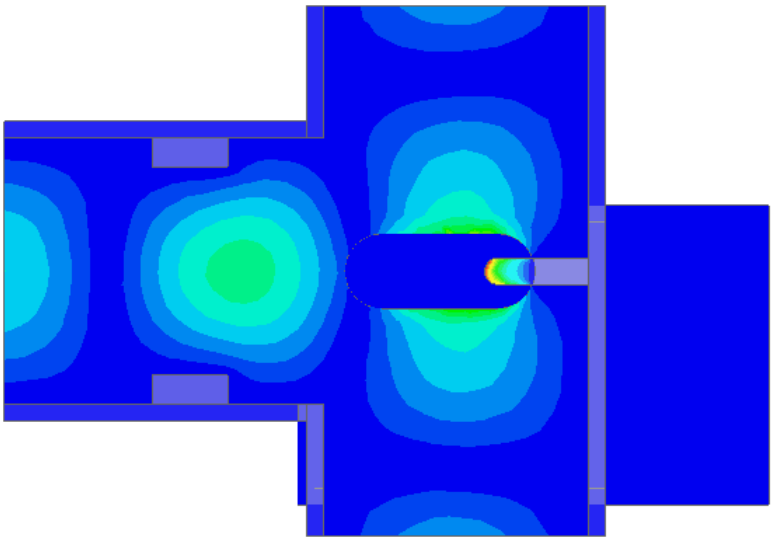

Figure 19: Power flow across Comparator Network

Table 7: Comparator network parameters

Parameter	**Value (mm)**
Length(L)	46.8
Width(w)	31.4988
Input Height(InH)	7.8994
Input Width(InW)	15.7988
Thickness(t)	1
Slot length(Cou L)	11
Slot width(Cou W)	4
Ir1 W	3.5
Ir1 H	7.8994
Ir2 W	6.5
Ir1 H	7.8994

3.3 Results

The monopulse comparator network for slot array antenna is designed and simulated using high frequency EM simulator HFSS[34]. Electrical performance of monopulse network is desired to meet the bandwidth and reflection coefficients requirements. It is to avoid any degradation in complete antenna performance after interface of comparator network with antenna.

It is desired that comparator network should cover frequency range from 14.4 GHz to 15.35 GHz. Both, sum and difference ports cover the desired impedance bandwidth of 950 MHz. Sum & difference port have 3 GHz and 1300 MHz impedance bandwidth respectively. In the design of comparator network, it is required that both ports should be isolated enough to avoid any degradation in performance due to coupling. Isolation between ports is greater than 40 dB. Reflection coefficients of sum and delta ports are shown in Fig. 20. Isolation between both ports is shown in Fig.21.

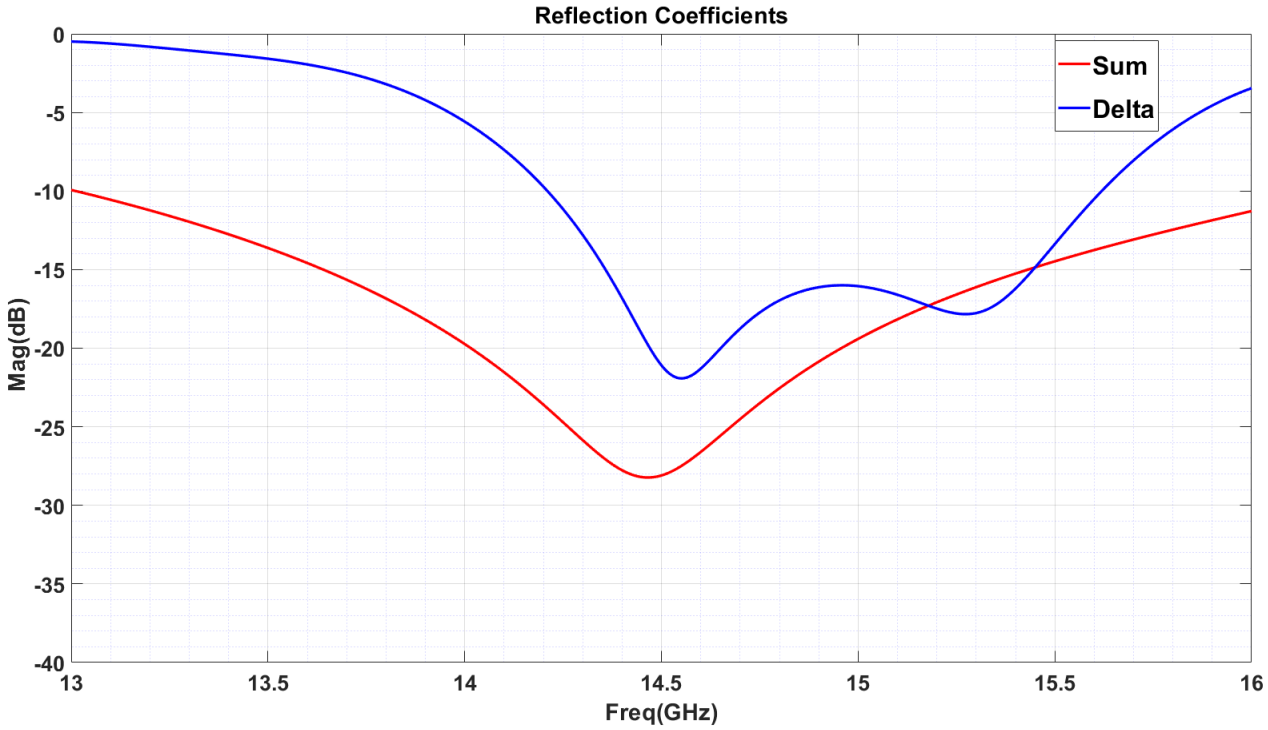

Figure 20: Input reflection coefficients of comparator

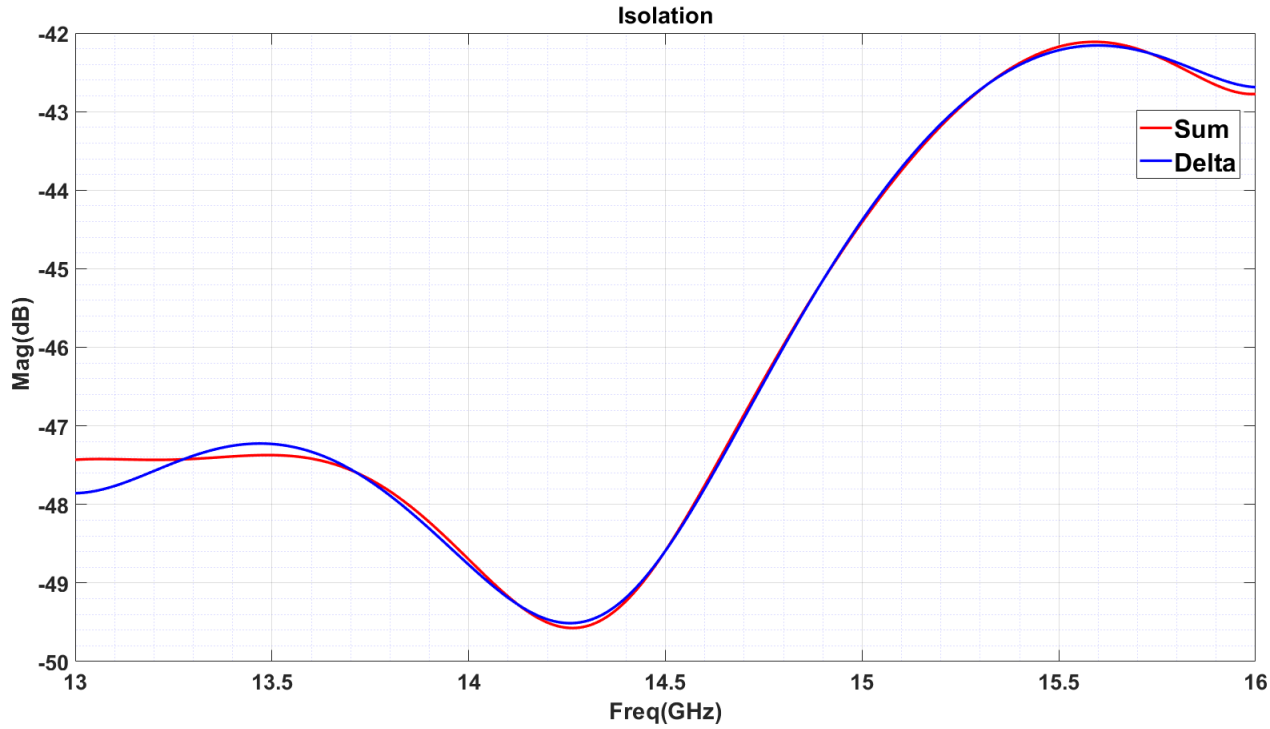

Figure 21: Isolation between sum and difference ports of comparator

CHAPTER IV

MONOPULSE ANTENNA RESULTS

The complete antenna structure is designed and modelled in two phases. In first phase, a slotted waveguide array is designed and simulated using HFSS. In second phase , a bilayer monopulse comparator network is designed and integrated with antenna to get the desired sum and difference pattern. The monopulse feed network has higher bandwidth as compared to the slot array. However, integrated antenna covers the desired impedance bandwidth.

4.1 Results

The integrated antenna structure is compact having dimensions of 10.8 cm x 10.7 cm x 4 cm that makes it easy to fit on-board. Exploded view of the complete antenna structure explaining different components is shown in Fig. 22. The designed antenna has higher impedance bandwidth of 8% at 15 GHz i.e $>$ 1200 MHz for sum and difference ports. The reflection coefficient plot for integrated antenna structure is shown in Fig. 23. Both ports have isolation better than -40 dB. Sum and difference port isolation is shown in Fig.24. Gain at designed frequency is 22.5 dB and is greater than 20.5 dB in the desired frequency range. The far-field plot at 15 GHz exhibiting sum and difference pattern in Phi= 0° plane is shown in Fig.25. It has lobe level less than -13 dB and null depth for difference pattern is more than 30 dB. The 3dB beam-width is 9.3° and 10.8° in azimuth and elevation plane respectively.

The sum radiation pattern in all three principal planes ($\phi = 0°, \phi = 45°$ and $\phi = 90°$) at three different frequencies i.e: 14.4 GHz, 14.9 GHz and 15.4 GHz is shown in Fig. 26. The difference radiation pattern in azimuth plane ($\phi = 0°$) at three different frequencies i.e: 14.4 GHz, 14.9 GHz and 15.4 GHz is shown in Fig.27.3D

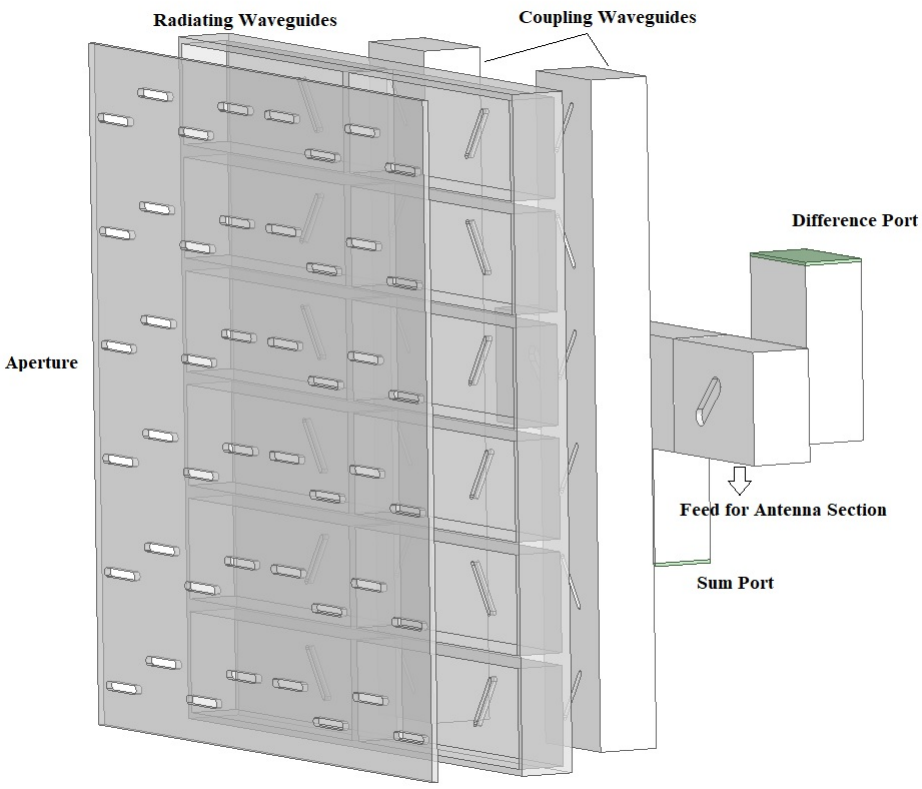

Figure 22: Integrated antenna structure

polar plot at three different frequencies i.e: 14.4 GHz, 14.9 GHz and 15.4 GHz is shown in Fig.28.

4.2 Conclusion

A compact, low-profile, high impedance bandwidth and high gain slotted waveguide array with monopulse capability for airborne radio applications is presented. The reflection bandwidth of whole system is 8% of the design frequency 15 GHz that is greater than the commercially available products like in [17]. It has high gain greater than 22.5 dB , SLL ≤ -13 dB and 3-dB beam-width of 9.3° in Az-plane and 10.3° in El-plane at 15 GHz.The gain of antenna is maximum at 14.8 GHz and slightly degrades towards the end of the bandwidth. However, it is greater than 20 dB from 14.4 GHz - 15.35 GHz as per link budget requirements.

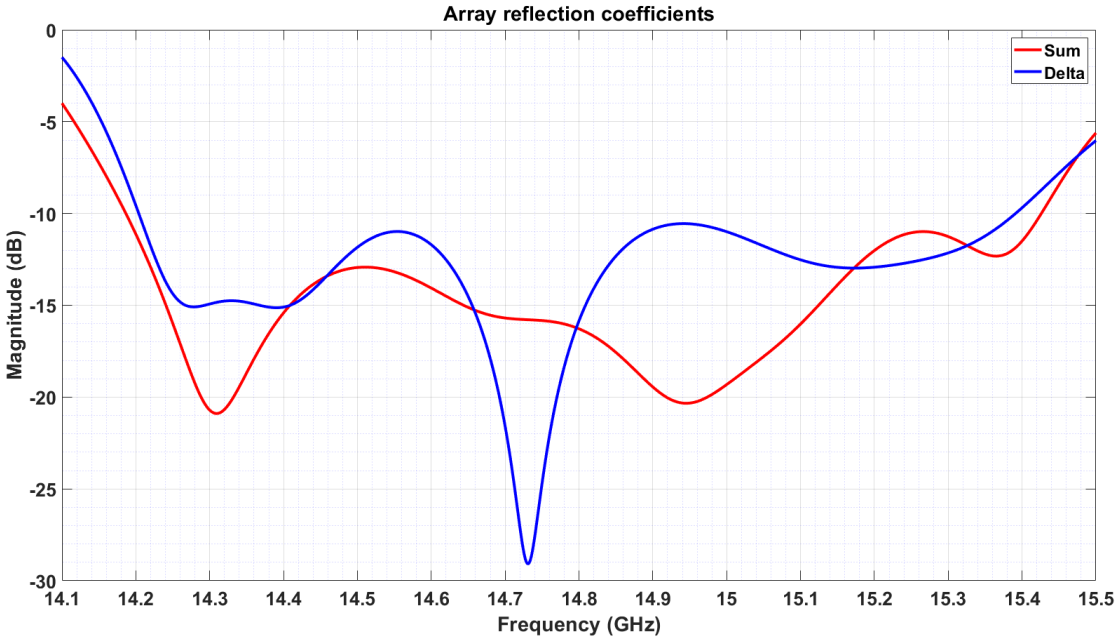

Figure 23: Reflection coefficient of sum and delta port

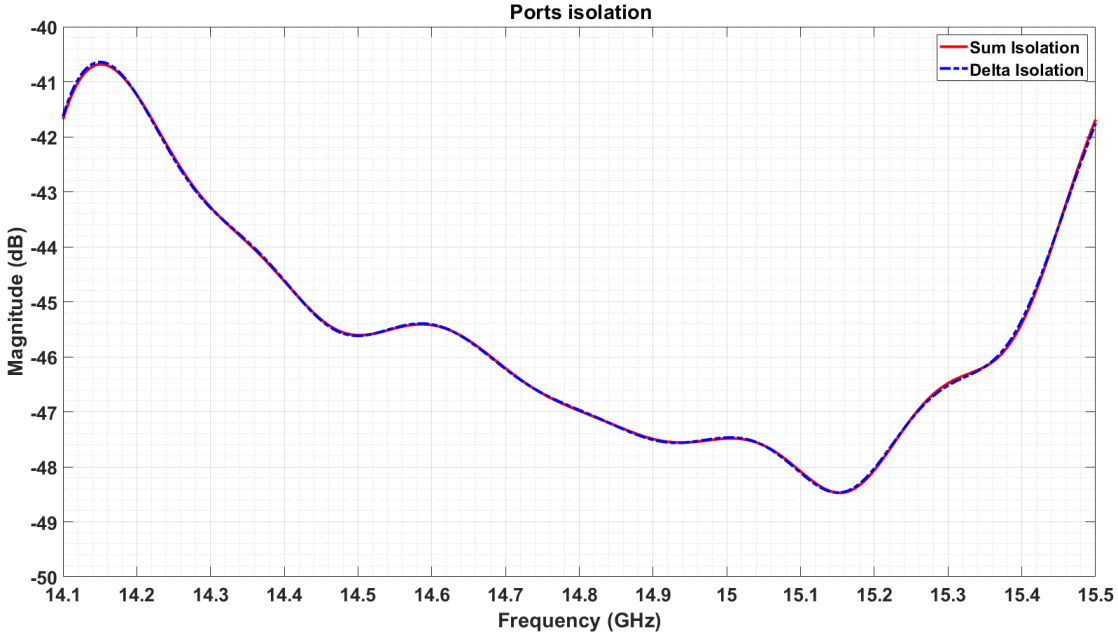

Figure 24: Sum and difference port Isolation of complete structure

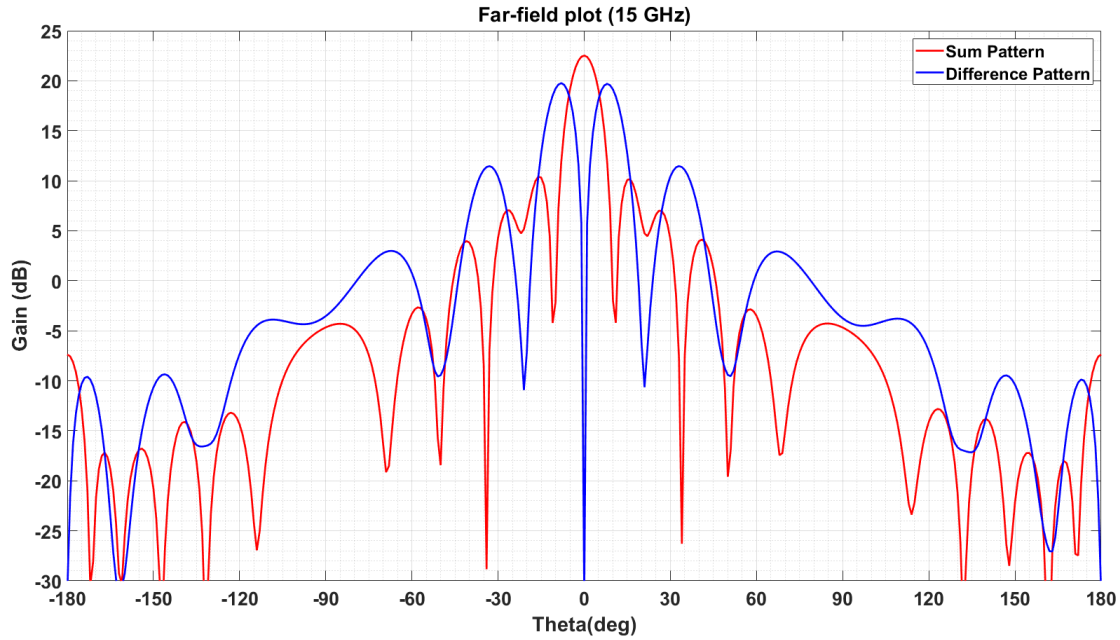

Figure 25: Far-field plot at 15 GHz

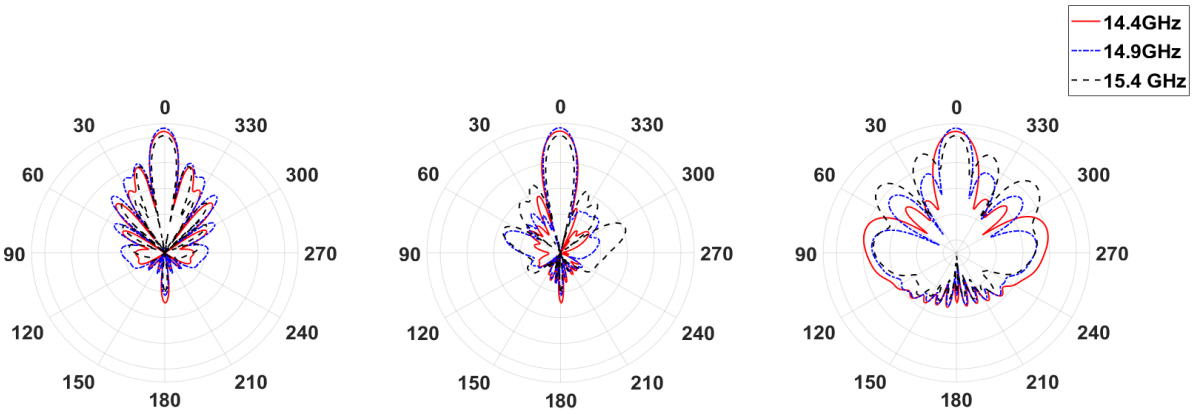

Figure 26: Sum radiation pattern in three principal planes

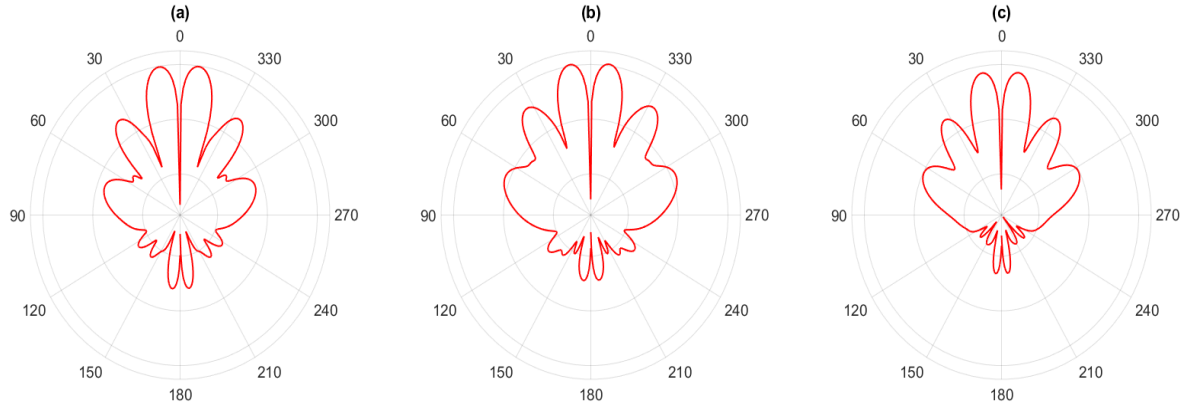

Figure 27: Difference radiation pattern (a) 14.4 GHz, (b) 14.9 GHz and (c) 15.4 GHz

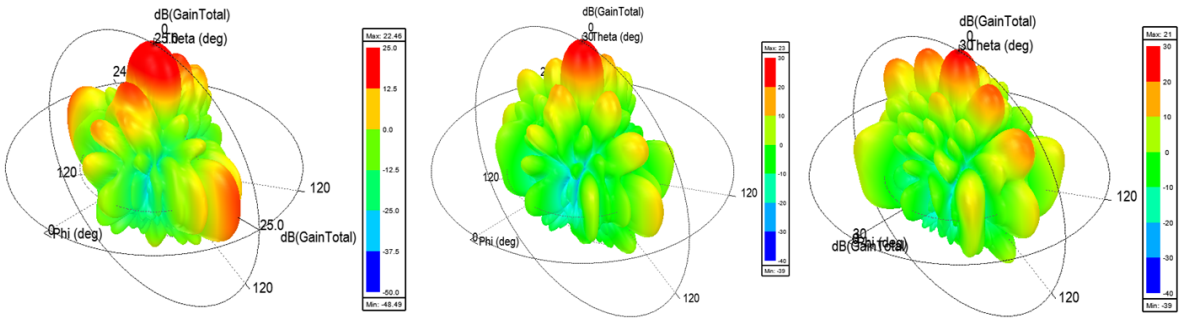

Figure 28: 3D polar plot (a) 14.4 GHz, (b) 14.9 GHz and (c) 15.4 GHz

CHAPTER V

POLARIZER

In order to avoid any losses due to polarization mismatch due to geometrical rotation of either transmitting or receiving antenna, it is desired to obtain maximum data performance of onboard communication system in airborne and spaceborne applications. In the past few years, different methods have been proposed to improve the data throughput of onboard communication system by means of frequency reuse or polarization utilization[43, 44]. In [45] Baunge et.al proposed a method to reuse polarization by using strip of metallic wires to separate signals.

Many structures have been proposed to obtain circular polarization from a linearly polarized incident wave. Pierrot [46] presented first design based on an array of wires with a bandwidth of 10%. Tilston in [47] presented a circular polarization selective surface based on conducting wires. Another design based on resonant spirals was presented by Morin[48]. All the mentioned structures are classical resonant designs with very narrow bandwidth. D. Sjoberg [49] presented a non-resonant multi-layer circular polarization structure with higher bandwidth and smaller physical size($0.68\lambda_\circ$).

In this research, a non-resonant linear to circular polarization converter based on meander lines and conducting wires on thin sheets that are stacked together is presented. The proposed structure is smaller in physical size($0.59\lambda_\circ$) and is low-cost as compared to the designs mentioned above. The designed polarizer can be easily integrated with the monopulse slot array by just simply mounting on top of the array. The different layers of polarizer are separated by a low-permittivity material called spacer or foam. It is also used to mount the polarizer on the antenna aperture.

5.1 Polarizer Design

The design of polarizer is based on unit cell approach simulated using Floquet's theorem which states that in a given mode and at a given frequency, the electromagnetic fields at any pair of corresponding points separated by a certain period are related by the same constant factor. The unit cell is multilayer structure of thin substrates having conducting strips and meander lines. Each layer is separated by a spacer having thickness of $\lambda_\circ/8$ and is rotated 45° with respect to previous layer. The linear to circular polarization structures presented in [49] is wideband covering whole Ku-band but is quite expensive to manufacture because of using very thin(0.127mm) low-permittivity substrates. The desired application of this research only needs to cover 14.4-15.35 GHz part of Ku-band. Therefore, a low cost design is presented by trading off impedance bandwidth. However, this research covers the desired bandwidth.

The 3D model of unit cell is shown in Fig.29. The design is based on hybrid approach utilizing metallic strips and meander lines to achieve circular polarization from incident linearly polarized wave. The width of strip lines, width, height and period of the meander lines and spacing between each layer are basic design parameters.

Response of thin conducting lines parallel to electric field is inductive and stronger than lines orthogonal to the electric field which have capacitive response. As meander line is based on lines parallel and orthogonal to electric field, therefore scattering matrix for the circular polarization meander line contains both linear components i.e: parallel and orthogonal. If $r^{\parallel}$ and $r^{\perp}$ are the parallel and orthogonal linear components to the electric field respectively, scattering matrix [49] for circular polarization

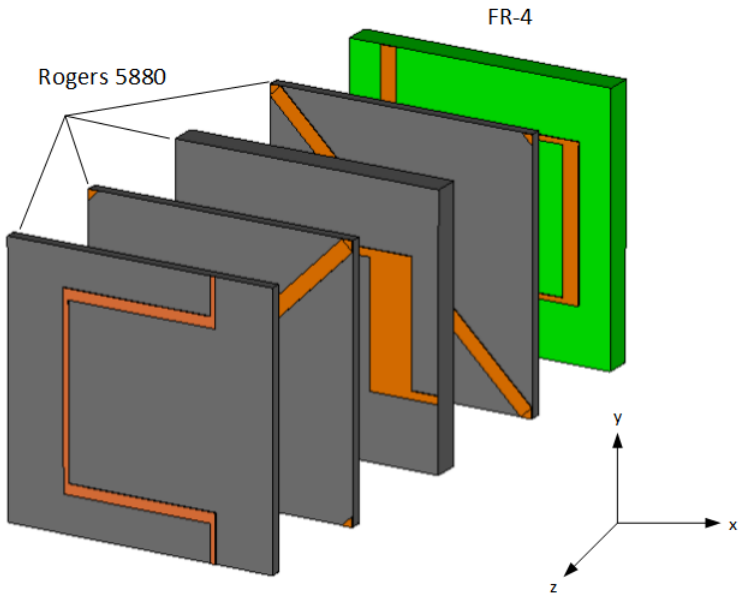

Figure 29: Unit cell of Linear to Circular Polarization converter

can be given by Eq.5

$$
\begin{aligned}
S^{CP} &= \begin{pmatrix} S_{11}^{RR} & S_{11}^{RL} & S_{12}^{RR} & S_{12}^{RL} \\ S_{11}^{LR} & S_{11}^{LL} & S_{12}^{LR} & S_{12}^{LL} \\ S_{21}^{RR} & S_{21}^{RL} & S_{22}^{RR} & S_{22}^{RL} \\ S_{21}^{LR} & S_{21}^{LL} & S_{22}^{LR} & S_{22}^{LL} \end{pmatrix} \\
&= \begin{pmatrix} 0 & 0 & 1 & 0 \\ 0 & 0 & 0 & 1 \\ 1 & 0 & 0 & 0 \\ 0 & 1 & 0 & 0 \end{pmatrix} + \frac{r^{\parallel} + r^{\perp}}{2} \begin{pmatrix} 0 & 1 & 1 & 0 \\ 1 & 0 & 0 & 1 \\ 1 & 0 & 0 & 1 \\ 0 & 1 & 1 & 0 \end{pmatrix} \\
&\quad + \frac{r^{\parallel} - r^{\perp}}{2} \begin{pmatrix} e^{2j\phi} & 0 & 0 & e^{2j\phi} \\ 0 & e^{-2j\phi} & e^{-2j\phi} & 0 \\ 0 & e^{-2j\phi} & e^{-2j\phi} & 0 \\ e^{2j\phi} & 0 & 0 & e^{2j\phi} \end{pmatrix}
\end{aligned} \tag{5}
$$

where superscripts RR and LL represents the co-pol reflection co-efficient for right hand and left hand circular polarization while RL and LR represents cross-polarization

co-efficient respectively. The angle ϕ is the angle of meander line with the horizontal axis of unit cell shown in Fig.29.

For practical design approximation, wave propagating between two meander lines printed on dielectric substrate and separated by distance "d "must experience a propagation delay. Therefore, taking this into account, single parameter approximation can be done to select between right and left hand circular polarization. This approximation [49] is given by Eq.6

$$\begin{aligned} S_{11}^{RR} &\approx \frac{r^{\parallel} - r^{\perp}}{2}(1 + e^{-2jkd}e^{2j\phi}) \\ S_{11}^{LL} &\approx \frac{r^{\parallel} - r^{\perp}}{2}(1 + e^{-2jkd}e^{-2j\phi}) \\ S_{11}^{LR} &\approx \frac{r^{\parallel} + r^{\perp}}{2}(1 + e^{-2jkd}) \\ S_{21}^{RR} &\approx \frac{r^{\parallel} + r^{\perp}}{2}(1 + e^{-2jkd}) \end{aligned} \tag{6}$$

where "k"is the free space wave-number. In order to get the right hand circular polarization(RHCP), S_{11}^{RR} can be maximized by choosing $\phi = \pi/4$ that can also results in minimizing S_{11}^{LL}. Similarly, $\phi = -\pi/4$ can maximize S_{11}^{LL} , minimizing S_{11}^{RR} and giving left hand circular polarization (LHCP). The addition of two more substrate layers reduces the cross polarization reflection co-efficient. Therefore, theoretically four layers of metallic strips on dielectric substrates separated by certain distance is sufficient to transmit one polarization and reflect the other. But in reality, metallic strip are strop interacting because of thin substrates. Therefore, one more substrate layer is added to achieve the good polarization.

The initial meander line model parameters and strip line width are calculated by using a classical analytical model explained in [50]. These parameters are then used to model a basic unit cell shape in HFSS and simulated using Floquet ports. Unit cell simulation can help to get the desired results for an array of any length in a very small computation time. As mentioned earlier, meander lines are printed on very

thin substrates but it increases cost of the polarizer. Meander lines on different layers are generally same just rotated by $\phi = 45°$ with respect to previous layer. Meander lines in three layers are different because the thickness of substrates vary. 1^{st} layer is designed on FR-4 substrate with thickness of 0.508 mm, 2^{nd} meander line is designed on 0.508 mm thick substrate and third meander line is designed on 0.203 mm thick substrate.Metallic strips along diagonal are etched on 0.203 mm thick substrate. The materials used in design are summarized in Table.8. Different geometrical parameters of meander lines illustrated in Fig.30 are given in Table.9

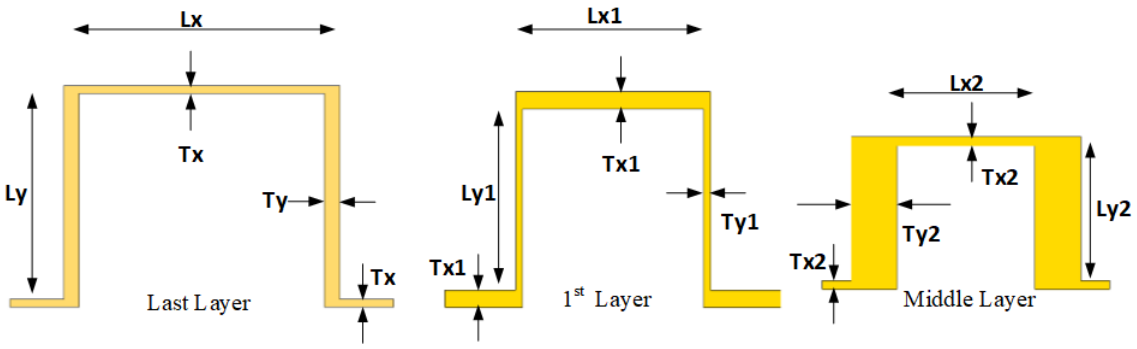

Figure 30: Meander lines used in polarizer design

Table 8: Materials used in polarizer design

Material	Thickness(mm)	Permittivity
FR-4	0.508	$\epsilon_r = 4.3$
Rogers(5880)	0.508	$\epsilon_r = 2.2$
Rogers(5880)	0.203	$\epsilon_r = 2.2$
Spacers (Rohacel HF51)	2.5	$\epsilon_r = 1.067$

5.2 Results

The designed unit cell is simulated in HFSS using Floquet modes concept[52]. In order to achieve circular polarization from polarizer, electric field must be divided equally among the parallel and orthogonal linear components. Zmin(1),Zmax(1) and

Table 9: Geometrical parameters of meander lines

Parameter	**Value(mm)**
Tx	0.1
Ty	0.3
Lx	2.7
Ly	3.1
Tx1	0.3
Ty1	0.1
Lx1	2.8
Ly1	3.1
Tx2	0.15
Ty2	0.7
Lx2	2.4
Ly2	2.5

Zmin(1),Zmax(2) represents linear of electric field i.e parallel and perpendicular. The linear modes of electric field should be close to -3dB with phase difference close to -90° which means field is equally divided between two orthogonal modes . Initially, only unit cell is designed and simulated and later this unit cell is converted to an array of the length of antenna aperture. This array is mounted on the top of antenna using low permittivity material Rohacel HF31.

5.3 Unit cell results

The magnitude of orthogonal modes is shown in Fig.31.The two linear modes of polarizer represented by Zmin(1),Zmax(1) and Zmin(1),Zmax(2) are -3.45 dB and -3.46 dB respectively at 15 GHz. This means insertion loss for the designed polarizer is 0.46 dB in the frequency range of interest. Phase difference is shown in Fig.32. The phase difference is 87° at 15 GHz and is close to 90° in desired bandwidth.

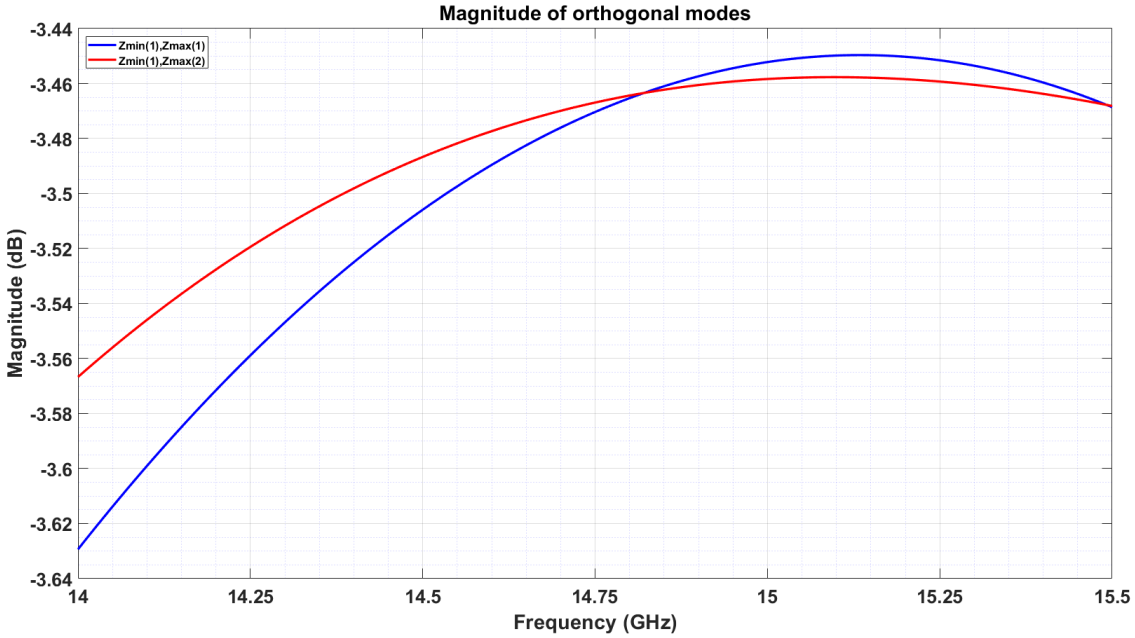

Figure 31: Magnitude of orthogonal modes

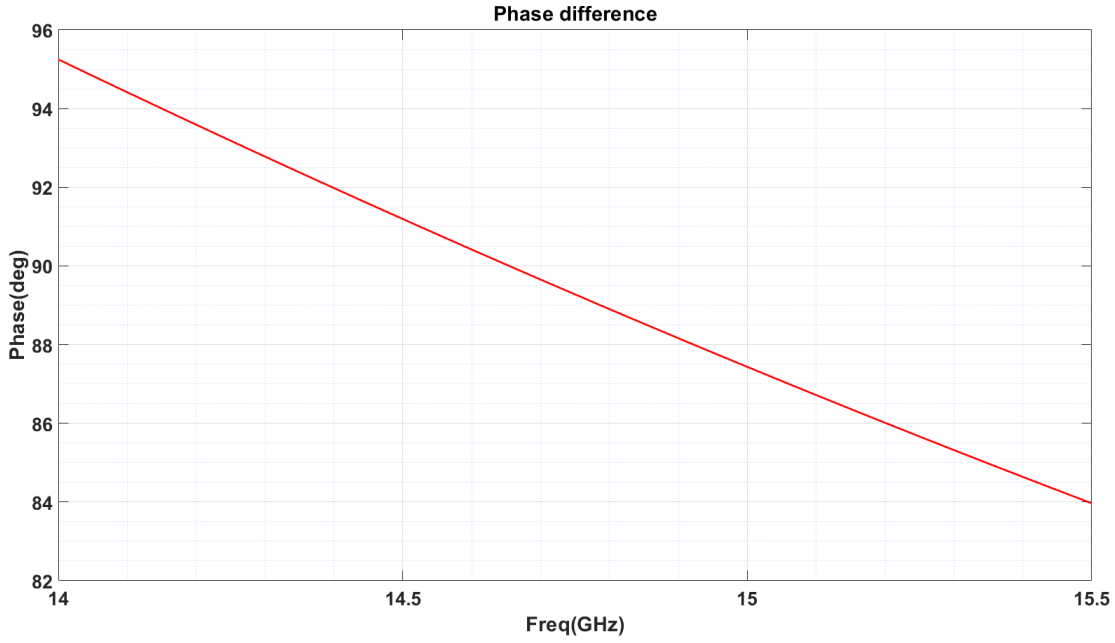

Figure 32: Phase difference between orthogonal modes

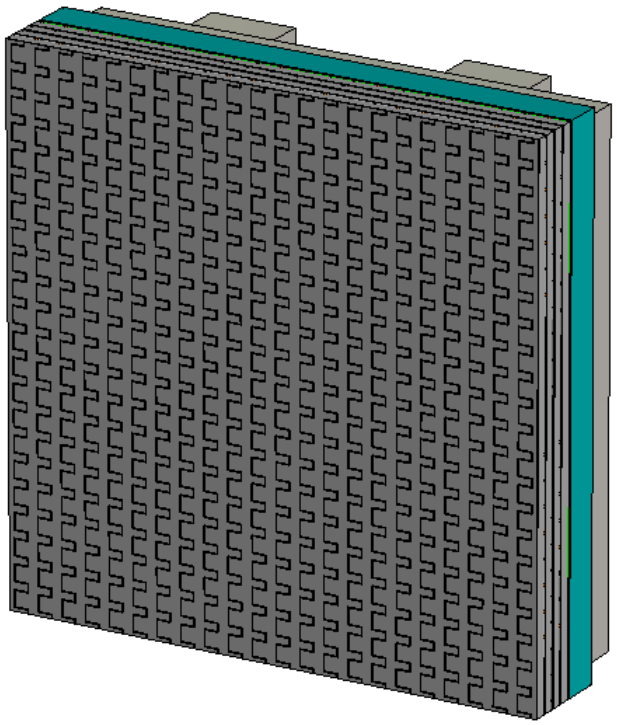

Figure 33: 3D model of complete system

5.4 System results

The designed unit cell is extended to an array of dimensions 110 cm x 110 cm and integrated with mono-pulse slotted wave-guide array. The polarizer array is placed at distance of $3\lambda/8$ i.e: 7.5 mm from antenna aperture. 3D model of antenna integrated with polarizer is shown in Fig.33.

Reflection coefficients are shown in Fig.34. It can be observed that antenna impedance is matched with that of sum and difference port . The reflection coefficients of the complete system are slightly better than antenna only. It is because of adding dielectric layers on the top of the antenna aperture. Axial ratio is the measure of ratio between major and minor axis of the polarization ellipse. The axial ratio is 0 dB ideally but it desired to be less than 3 dB for realistic circular polarized antennas. Axial ratio over the entire bandwidth is shown in Fig.37. The presented antenna has

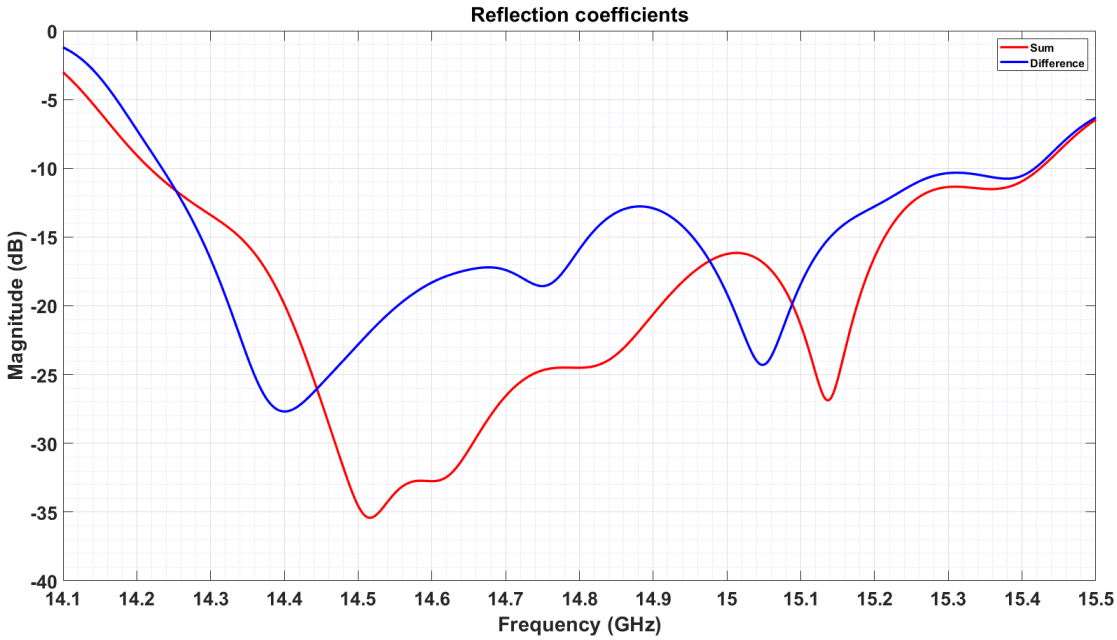

Figure 34: Reflection coefficients of complete system

excellent axial ratio less than 1.5 dB in two planes i.e : Phi=0° and Phi=45°. It is less than 2.5 dB for Phi=90° plane. Nevertheless, it is better than desired value of 3 dB.

The far-field plot at 15 GHz exhibiting sum and difference pattern in Phi= 0° plane is shown in Fig.35. The antenna cross polarization plot is shown in Fig. 36. The sum patterns in three principal planes are shown in Fig.38. Difference radiation pattern for three frequencies i.e: 14.4 GHz, 14.9 GHz and 15.4 GHz is shown in Fig.39.

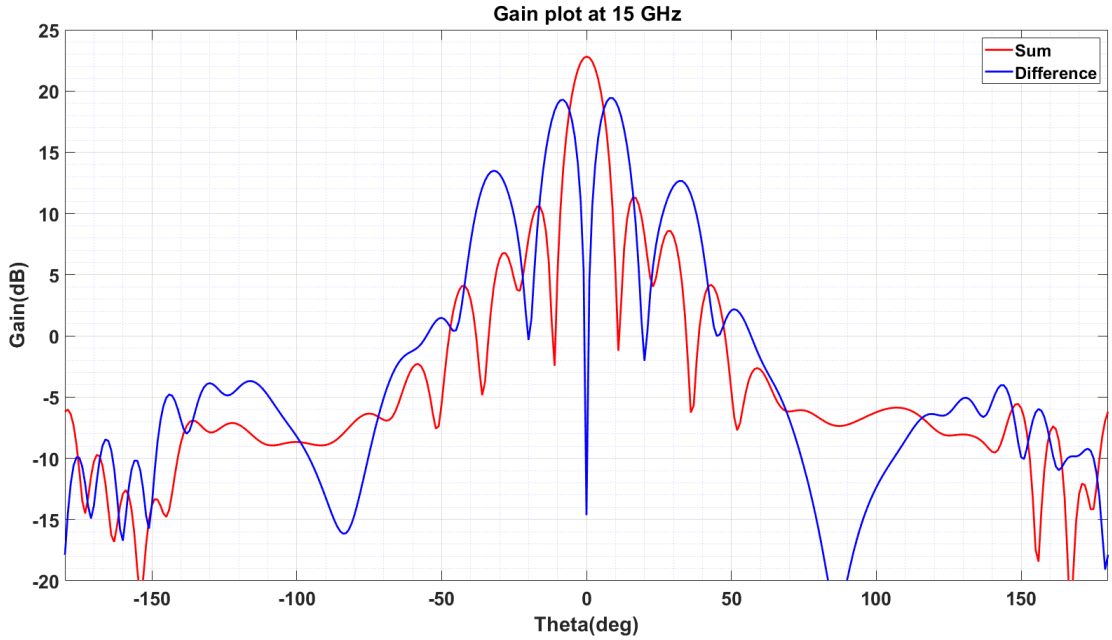

Figure 35: Far-field pattern of complete system at 15 GHz

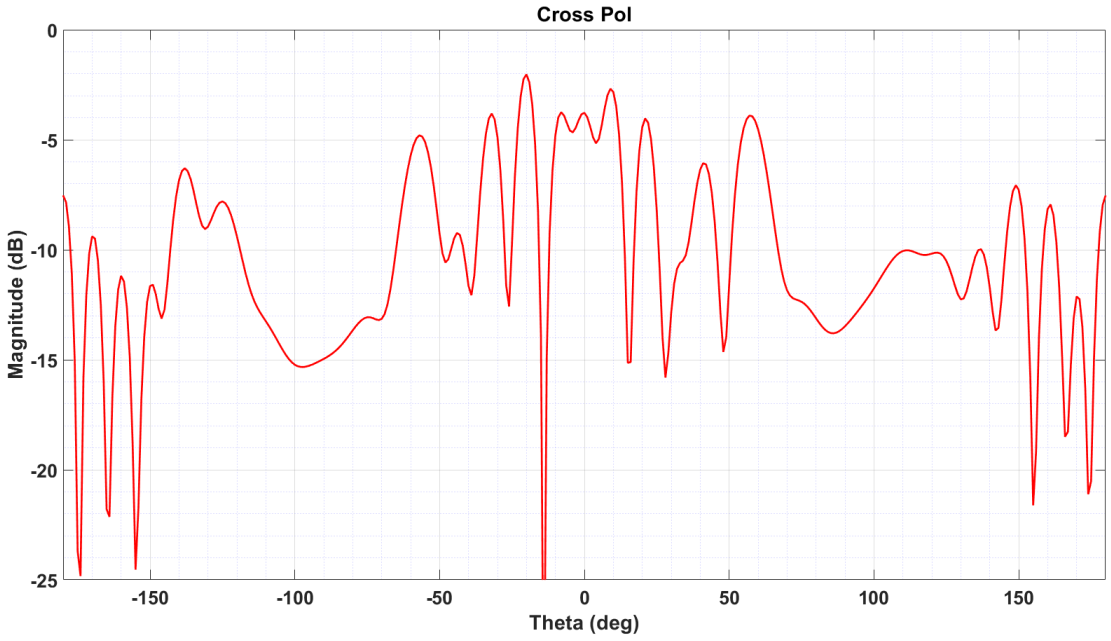

Figure 36: Cross polarization of complete system at 15 GHz

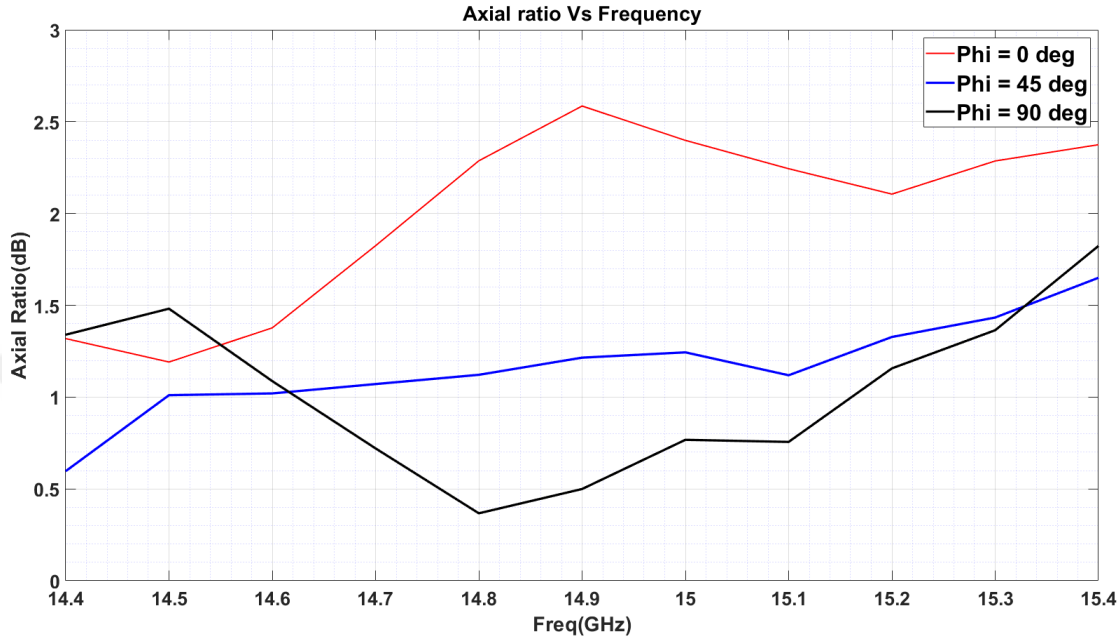

Figure 37: Axial ratio over the entire bandwidth

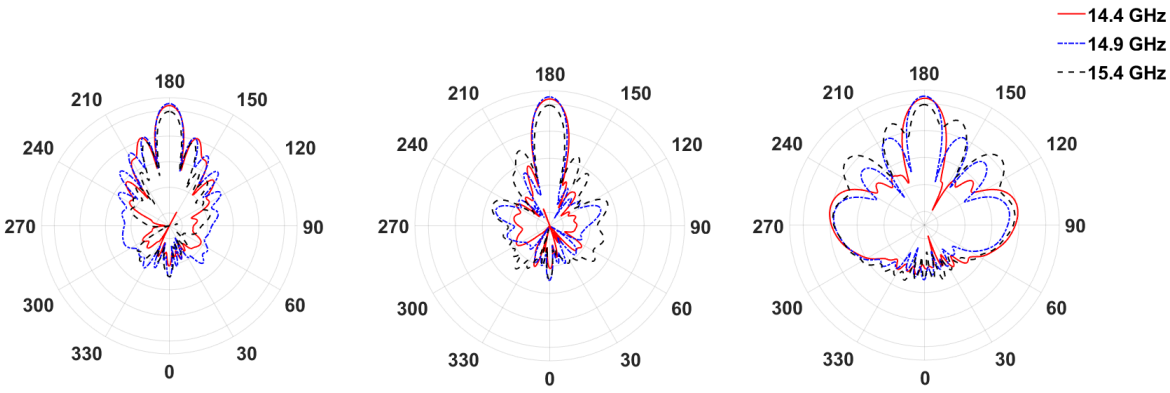

Figure 38: Sum radiation pattern in three principal planes for whole system

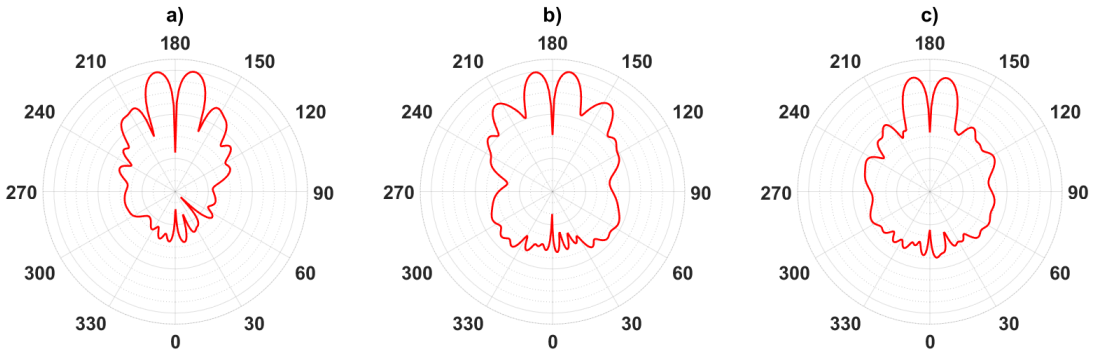

Figure 39: Difference radiation pattern for whole system a) 14.4 GHz , b) 14.9 GHz and c) 15.4 GHz

CHAPTER VI

CONCLUSION AND FUTURE WORK

In this thesis, a circularly polarized slot array antenna with single plane monopulse capability is presented. Antenna is designed for RF LOS communications for MALE UAVs. The aim of presented design is to cover the uplink and downlink frequency band to perform command, control and communications (C3) operation that includes TTC & payload data transfer. All the requirements related to antenna electrical performance laid by link budget calculations are met efficiently. The antenna is compact enough to easily integrate on board.

According to link budget given in Table.1, it is desired to have an antenna gain of 20 dB. The designed antenna has a simulated gain of 22.5 dB at centre frequency of 15 GHz. It has gain greater than 20 dB in desired frequency band (14.4 -15.35 GHz). The required impedance bandwidth for targeted application is 950 MHz to cover uplink and downlink frequency range but presented antenna has impedance bandwidth greater than 1200 MHz. Higher gain and impedance bandwidth than required provides an extra margin for tolerance in manufacturing.

In order to avoid any polarization mismatch losses , antenna is desired to have circular polarization. Slotted waveguide arrays are inherently linearly polarized array. Therefore, circular polarization is achieved using a multi layer meander line polarizer placed on top of the antenna. Antenna is designed for azimuth plane monopulse capability because when UAV attains its flying altitude of 15,000-20,000 feet at certain distance away from ground station, elevation plane monopulse is not required. The axial ratio in all three planes is less than 3 dB for the designed antenna. Antenna components can be manufactured separately and assembled easily. Slots are designed

with round slot corners for ease of manufacturing. The aperture can be manufactured separately with just 1 mm thickness aluminium sheet. The complete structure including polarizer has maximum dimensions of 10.8 cm x 10.7 cm x 9.2 cm.

The future work includes the bandwidth enhancement by improving reflection coefficient of the antenna. Although, gain requirements are met according to link budget but in future design, gain flatness with respect to frequency will be improved.Sidelobe level (SLL) will be further enhanced in the future by using amplitude tapering instead of uniform tapering. SLL for Phi=90° plane towards the end of band i.e. 15.35 GHz is -9 dB instead of -13 dB due to distortions in the standing wave array as we move away from design frequency. Therefore, it can be improved in the future design. Comparator network of the antenna can be extended for dual plane monopulse capability by adding third layer to get difference pattern in elevation plane as well. Polarizer will be further improved to reduce insertion loss and to achieve better axial ratio for Phi=90° plane. For a very short duration, UAV will not have line of sight communication with ground control station. An omni-directional antenna can be added with this array for that narrow time slot.

Bibliography

[1] M. Erdelj, E. Natalizio, K. R. Chowdhury, and I. F. Akyildiz, "Help from the sky: Leveraging uavs for disaster management," *IEEE Pervasive Computing*, vol. 16, no. 1, pp. 24–32, 2017.

[2] S. Hayat, E. Yanmaz, and R. Muzaffar, "Survey on unmanned aerial vehicle networks for civil applications: A communications viewpoint," *IEEE Communications Surveys & Tutorials*, vol. 18, no. 4, pp. 2624–2661, 2016.

[3] J. M. Sullivan, "Evolution or revolution? the rise of uavs," *IEEE Technology and Society Magazine*, vol. 25, no. 3, pp. 43–49, 2006.

[4] R. Luppicini and A. So, "A technoethical review of commercial drone use in the context of governance, ethics, and privacy," *Technology in Society*, vol. 46, pp. 109–119, 2016.

[5] K. B. Sandvik and K. Lohne, "The rise of the humanitarian drone: giving content to an emerging concept," *Millennium*, vol. 43, no. 1, pp. 145–164, 2014.

[6] H. Voemel, C. Wolff, S. Oncley, J. A. Moore, S. M. Ellis, and D. Axisa, "Outcomes of the ncar/eol workshop unmanned aircraft systems for atmospheric research," in *AGU Fall Meeting Abstracts*, 2018.

[7] İ. Çuhadar and M. Dursun, "Unmanned air vehicle systems data links," *Journal of Automation and Control Engineering*, vol. 4, no. 3, 2016.

[8] C. Malveaux, S. Hall, and R. Price, "Using drones in agriculture: unmanned aerial systems for agricultural remote sensing applications. 2014 asabe and csbe," in *SCGAB annual international meeting sponsored by ASABE*, 2014.

[9] C. Luo, J. Nightingale, E. Asemota, and C. Grecos, "A uav-cloud system for disaster sensing applications," in *2015 IEEE 81st Vehicular Technology Conference (VTC Spring)*, pp. 1–5, IEEE, 2015.

[10] W. Zhang and J. Wu, "To explore the uav application in disaster prevention and reduction," in *Applied Mechanics and Materials*, vol. 590, pp. 609–612, Trans Tech Publ, 2014.

[11] M. Hassanalian and A. Abdelkefi, "Classifications, applications, and design challenges of drones: A review," *Progress in Aerospace Sciences*, vol. 91, pp. 99–131, 2017.

[12] M. Arjomandi, S. Agostino, M. Mammone, M. Nelson, and T. Zhou, "Classification of unmanned aerial vehicles," *Report for Mechanical Engineering class, University of Adelaide, Adelaide, Australia*, 2006.

[13] S. G. Gupta, M. M. Ghonge, and P. Jawandhiya, "Review of unmanned aircraft system (uas)," *International journal of advanced research in computer engineering & technology (IJARCET)*, vol. 2, no. 4, pp. 1646–1658, 2013.

[14] E. Gutiérrez Fernández, "Management system for unmanned aircraft systems teams," Master's thesis, Universitat Politècnica de Catalunya, 2010.

[15] T. J. Osborn, "A review of unmanned aerial vehicle designs and operational characteristics," in *NARCAP TR-11*, 2009.

[16] M. E. Grisworld, "Spectrum management: Key to the future of unmanned aircraft systems?(maxwell paper, number 44)," tech. rep., AIR WAR COLL MAXWELL AFB AL, 2008.

[17] "CPII at-20 directional antenna." `https://www.cpii.com/docs/datasheets/393/AT-20%20%202-9-15.pdf`. Accessed: 2019-10-08.

[18] T. Li, H. Meng, and W. Dou, "Design and implementation of dual-frequency dual-polarization slotted waveguide antenna array for ka-band application," *IEEE Antennas and Wireless Propagation Letters*, vol. 13, pp. 1317–1320, 2014.

[19] Y.-Q. Wen, B.-Z. Wang, and X. Ding, "Wide-beam siw-slot antenna for wide-angle scanning phased array," *IEEE Antennas and Wireless Propagation Letters*, vol. 15, pp. 1638–1641, 2016.

[20] H. Bayer, A. Krauss, R. Stephan, and M. A. Hein, "Compact ka-band cassegrain antenna with multimode monopulse tracking feed for satcom-on-the-move applications," in *2016 10th European Conference on Antennas and Propagation (EuCAP)*, pp. 1–5, IEEE, 2016.

[21] S. R. Rengarajan, "Theory of a traveling wave feed for a planar slot array antenna," in *2011 XXXth URSI General Assembly and Scientific Symposium*, pp. 1–4, IEEE, 2011.

[22] W. H. Watson, "Resonant slots," *Journal of the Institution of Electrical Engineers - Part IIIA: Radiolocation*, vol. 93, no. 4, pp. 747–777, 1946.

[23] A. Stevenson, "Theory of slots in rectangular wave-guides," *Journal of Applied Physics*, vol. 19, no. 1, pp. 24–38, 1948.

[24] R. Elliott and L. Kurtz, "The design of small slot arrays," *IEEE Transactions on Antennas and Propagation*, vol. 26, no. 2, pp. 214–219, 1978.

[25] R. Elliott, "On the design of traveling-wave-fed longitudinal shunt slot arrays," *IEEE Transactions on Antennas and Propagation*, vol. 27, no. 5, pp. 717–720, 1979.

[26] M. Orefice and R. Elliott, "Design of waveguide-fed series slot arrays," in *IEE Proceedings H (Microwaves, Optics and Antennas)*, vol. 129, pp. 165–169, IET, 1982.

[27] H. Yee and P. Richardson, "Slotted waveguide antenna arrays," *IEEE Antennas and Propagation Society Newsletter*, vol. 24, no. 6, pp. 4–8, 1982.

[28] R. Elliott, "An improved design procedure for small arrays of shunt slots," *IEEE Transactions on Antennas and Propagation*, vol. 31, no. 1, pp. 48–53, 1983.

[29] L. Josefsson, "Analysis of longitudinal slots in rectangular waveguides," *IEEE Transactions on Antennas and Propagation*, vol. 35, no. 12, pp. 1351–1357, 1987.

[30] M. Muller, I. Theron, and D. Davidson, "Improving the bandwidth of a slotted waveguide array by using a centre-feed configuration," in *1999 IEEE Africon. 5th Africon Conference in Africa (Cat. No. 99CH36342)*, vol. 2, pp. 1075–1080, IEEE, 1999.

[31] R. A. Gilbert and J. Volakis, "Waveguide slot antenna arrays," *Antenna Engineering Handbook*, pp. 9–14, 2007.

[32] A. O. Salman, "A linearly slotted waveguide antenna and comparison of it with a sinusoidal one," 2013.

[33] J. Coetzee, J. Joubert, and W. Tan, "Frequency performance enhancement of resonant slotted waveguide arrays through the use of wideband radiators or sub-arraying," *Microwave and optical technology letters*, vol. 22, no. 1, pp. 35–39, 1999.

[34] ANSYS®, "ANSYS HFSS," 2018.

[35] R. J. Mailloux, *Phased array antenna handbook*. Artech house, 2017.

[36] M. Skolnik, *Introduction to Radar Systems*. McGraw-Hill Education, 2002.

[37] Xin Zhang, P. Willett, and Y. Bar-Shalom, "Monopulse radar detection and localization of multiple targets via joint multiple-bin processing," in *Proceedings of the 2003 IEEE Radar Conference (Cat. No. 03CH37474)*, pp. 232–237, May 2003.

[38] S. M. Sherman and D. K. Barton, *Monopulse principles and techniques*. Artech House, 2011.

[39] F. Cao, D. Yang, J. Pan, D. Geng, and H. Xiao, "A compact single-layer substrate-integrated waveguide (siw) monopulse slot antenna array," *IEEE Antennas and Wireless Propagation Letters*, vol. 16, pp. 2755–2758, 2017.

[40] G.-L. Huang, S.-G. Zhou, T.-H. Chio, and T.-S. Yeo, "Two types of waveguide comparator for wideband monopulse antenna array application," in *2015 IEEE 5th Asia-Pacific Conference on Synthetic Aperture Radar (APSAR)*, pp. 264–266, IEEE, 2015.

[41] V. K. Chaudhary, P. Verma, and U. Balaji, "Field theory based cad of inductive iris waveguide filter," in *APMC 2001. 2001 Asia-Pacific Microwave Conference (Cat. No. 01TH8577)*, vol. 1, pp. 318–321, IEEE, 2001.

[42] G. Matthaei, L. Young, and E. Jones, "Microwave filters, impedance-matching networks, and coupling structures, artech house," *Inc., Dedham, MA*, 1980.

[43] M.-A. Joyal and J.-J. Laurin, "Design and analysis of a cascade circular polarization selective surface at k band," *IEEE Transactions on Antennas and Propagation*, vol. 62, no. 6, pp. 3043–3053, 2014.

[44] W. A. Imbriale, S. S. Gao, and L. Boccia, *Space antenna handbook*. John Wiley & Sons, 2012.

[45] M. Baunge, H. Ekström, P. Ingvarson, and M. Petersson, "A new concept for dual gridded reflectors," in *Proceedings of the Fourth European Conference on Antennas and Propagation*, pp. 1–5, IEEE, 2010.

[46] R. Pierrot, "Reflector for circularly polarized waves," Mar. 10 1970. US Patent 3,500,420.

[47] W. V. Tilston, S. E. Tilston, M. Tilston, D. Tilston, T. Tralman, *et al.*, "Polarization selective surface for circular polarization," Oct. 1 1991. US Patent 5,053,785.

[48] G. A. Morin, "A circular polarization selective surface made of resonant helices," tech. rep., DEFENCE RESEARCH ESTABLISHMENT OTTAWA (ONTARIO), 1995.

[49] D. Sjöberg and A. Ericsson, "A multi layer meander line circular polarization selective structure (mlml-cpss)," in *The 8th European Conference on Antennas and Propagation (EuCAP 2014)*, pp. 464–468, IEEE, 2014.

[50] R.-S. Chu and K.-M. Lee, "Analytical method of a multilayered meander-line polarizer plate with normal and oblique plane-wave incidence," *IEEE Transactions on Antennas and Propagation*, vol. 35, no. 6, pp. 652–661, 1987.

[51] W. Wang, S.-S. Zhong, Y.-M. Zhang, and X.-L. Liang, "A broadband slotted ridge waveguide antenna array," *IEEE transactions on antennas and propagation*, vol. 54, no. 8, pp. 2416–2420, 2006.

[52] J. Crisostomo, W. Costa, and A. Giarola, "Electromagnetic wave propagation in multilayer dielectric periodic structures," *IEEE transactions on antennas and propagation*, vol. 41, no. 10, pp. 1432–1438, 1993.